N6-Methyladenine DNA modification regulates pathogen virulence in nematodes

Authors: Dadong Dai[1,2]†, Shurong Zhang[1]†, Boyan Hu[1], Yayi Zhou[1], Simeng Cui[1], Jia Sun[1], Yali Zhang[1,2], Xueyu Wang[1], Shahid Siddique[2], Dexin Bo[1], Min Zhang[3], Valerie M Williamson[4], Haozhe Yao[1], Xinya Duan[1], Wentao Wu[5], Donghai Peng[1], Jinshui Zheng[1]*, and Ming Sun[1]*

Affiliations:

[1]National Key Laboratory of Agricultural Microbiology, Huazhong Agricultural University, Wuhan 430070, China; Hubei Hongshan Laboratory, Wuhan 430070, China.

[2]Department of Entomology and Nematology, University of California Davis, One Shields Avenue, Davis, CA 95616, USA.

[3]Wuhan Academy of Agricultural Sciences, Wuhan 430065, Hubei, China.

[4]Department of Plant Pathology and the Genome Center, University of California, Davis, CA 95616, USA.

[5]Key Laboratory of Agricultural Biodiversity and Pest Control, College of Plant Protection, Yunnan Agricultural University, Kunming, China.

*Ming Sun and Jinshui Zheng.

Email: m98sun@mail.hzau.edu.cn, jszheng@mail.hzau.edu.cn

Author Contributions: M.S., J. Z., and D. D. conceived the project. M. S., J. Z., D. D., and D. P. administration the project. M. S. acquisition the funding. D.D. designed the experiments. D. D., S. Z. performed the experiments. S. Z. purified the protein and performed the in vitro protein activity experiments. S. Z., S. C., and J. S. constructed the transgenic plants. D. D. collected the data and performed the data analysis. Y.Z. and B.H. performed the Dot blot and western blot experiments. D. D., S. Z., X. W., S. C., Y. Z., M. Z., B. H., X. D., and W. W. prepared the materials. D. D. wrote the manuscript, S. S., and V.M.W. revised the manuscript.

Competing Interest Statement: The authors declare that they have no competing interests.

This PDF file includes:

Main Text

Figures 1 to 6

†These authors contributed equally to this work.

Abstract

The study of the global regulatory mechanisms controlling pathogen virulence gene expression is key to understanding the underlying mechanisms of pathogenicity. 6mA plays a critical role in regulating gene expression in response to various environmental stresses, but its biological functions related to pathogen virulence remain largely unexplored. We report the widespread presence of 6mA across 17 isolates of nematodes, along with an exploration of the 6mA landscape in the genomes of six notorious agricultural pathogen root-knot nematodes (RKNs). Our results indicate that 6mA has a conserved “GAG” motif in different nematodes but exhibits different distribution patterns and effects on gene expression. The distribution of 6mA in transposable elements differs between polyploid and diploid nematodes, suggesting lineage-specific epigenetic regulation potentially associated with polyploidy. Importantly, we identified two potential 6mA demethylases, MiNMAD-1 and MiNMAD-2, and confirmed their catalytic activity and site. Subsequent host-induced gene silencing of minmad-1 resulted in a significant increase in plant resistance to three polyploid RKNs species. A detailed functional characterization revealed that knocking down minmad-1 impaired the expression patterns of various virulence genes in the parasitic stage, thereby decreasing the virulence of RKNs on hosts. Our findings suggest that 6mA demethylase may serve as an epigenetic marker linked to pathogen virulence, enhancing our understanding of RKN biology and providing novel resources for the development of RKN prevention and control strategies.

Significance Statement

6mA methyltransferase regulates the expression of virulence genes in certain pathogenic bacteria and plays a critical role in their infectivity. However, the regulation of virulence gene expression in eukaryotic pathogens, particularly plant pathogens, remains largely unexplored. Most studies on pathogen virulence have focused on the function of individual effectors, with limited research on the global regulation of virulence gene expression. Through an epigenetic study of plant-parasitic nematodes, we found that 6mA globally regulates the expression patterns of virulence genes in RKNs. Furthermore, we generated transgenic tobacco, tomato, and rice plants expressing dsRNA targeting the nematode demethylase and found that these transgenic plants exhibited significantly enhanced resistance to RKNs. Overall, 6mA demethylase could be an efficient target for controlling plant-parasitic nematodes.

Main Text

Introduction

The regulation of pathogen virulence gene expression is crucial for uncovering the mechanisms of pathogenicity. Current research primarily focuses on the functional analysis of individual virulence genes, while little is known about the broader mechanisms governing the global regulation of virulence gene expression in pathogens. DNA methylation is one of the earliest discovered DNA modification pathways, leading to changes in chromatin structure, DNA conformation, stability, and interactions with proteins, thereby controlling gene

expression(1, 2). The role of 6mA in controlling bacterial virulence has been well-documented. DNA adenine methylase (Dam) is a crucial factor in *Salmonella* virulence(3). Dam(-) mutants exhibit multiple virulence-related defects(4) and may regulate the expression of the effector SpoA and SopB, which has phosphoinositide phosphatase activity(5, 6). Moreover, Dam has also been reported to globally affect the expression of genes associated with the cariogenic potential in *Streptococcus* mutans(7). Additionally, 6mA methyltransferase regulates the expression of virulence genes in pathogenic bacteria responsible for pediatric osteoarticular infections and enterocolitis(8, 9), as well as the virulence of the opportunistic pathogen Pseudomonas aeruginosa, which causes both acute and chronic infections(10). Furthermore, 6mA affects the expression of Mga, a major transcriptional regulator of multiple virulence genes in *Streptococcus pyogenes*(11). In eukaryotes, there are limited reports of 6mA-regulated virulence genes in fungi. 6mA methyltransferase is critical for the virulence of plant pathogenic fungi *Cryphonectria parasitica*(12). However, most studies on the relationship between 6mA and pathogen virulence have primarily focused on animal pathogens, leaving the connection between 6mA and virulence in plant pathogens largely unexplored. Moreover, while most functional studies of 6mA have focused on 6mA methyltransferases, the functions of demethylases remain largely unknown.

Recently, DNA 6mA modification has been reported in an increasing number of eukaryotes including *Caenorahabiditis elegans*(13), *Bursaphelenchus xylophilus*(14), *Drosophila*(15), *Chlamydomonas reinhardtii*(16), fungi(17, 18), plant(19-21), and mammal(22). In eukaryotes, 6mA methylation can occur in either symmetric or asymmetric contexts. However, studies in *C. elegans* and other species have indicated that asymmetric 6mA methylation predominates, especially in gene bodies or transposon-related regions. In our analysis, we observed a similar pattern in RKNs, consistent with the prevalence of asymmetric 6mA distribution. It has been shown that eukaryotic 6mA is transmitted via a semiconservative mechanism(23) and is incorporated into mammalian genome by DNA polymerase(24, 25). Moreover, 6mA has been reported to be associated with disease onset(26-28), embryonic development(15), and responses to environmental stress(20, 29). As 6mA modulators, demethylases influences a variety of biological processes such as spawning(13), ovary development(15), DNA replication and repair(30), vascular calcification(31), fatty acid metabolism in humans and mice(28), and neurodevelopment(32). The function of 6mA demethylase in pathogen infection process has been preliminary reported in *Mucor lusitanicus*(33). However, many previously reported eukaryotes with high levels of 6mA were later found most data from mammals and many other eukaryotes was clearly shown to be erroneous, like originating from bacterial contamination(34). Therefore, controlling bacterial contamination is particularly critical in the detection of 6mA in eukaryotes.

Nevertheless, the mechanism by which 6mA regulates the parasitism of eukaryotic pathogens, particularly the connection between demethylases and virulence, remains to be established. Plant-parasitic nematodes (PPNs) cause devastating economic losses, exceeding $100 billion annually(35). Root-knot nematodes (RKNs) are the most damaging PPNs(36) and have received increasing attention due to their broad host spectrum and complex ploidy status(37). Infective second juveniles of RKNs enter the plants close to the root tip and migrate

118 intercellularly to reach the vascular cylinder where they establish several giant cells. These
119 giant cells are highly modified and are the only source of nutrients for nematode throughout
120 their lifecycle. A wide range of nematode effectors facilitate the establishment and functioning
121 of giant cells(38). Yet, the epigenetic regulation patterns of these effector genes remain largely
122 unexplored. Existing studies on RKNs epigenetics have primarily focused on histone
123 modifications(39-41) and microRNA(42). Homology analysis of methyltransferase and
124 demethylase suggest that the *Meloidogyne incognita* (Mi) lacks DNA 6mA modification(43),
125 raising questions about the presence of 6mA in the RKN genome. Alternatively, it is possible
126 that these enzymes have substantial sequence divergence from already known enzymes,
127 requiring further investigation.
128
129 In this study, after eliminating bacterial DNA contamination, we explored the presence of 6mA
130 in 17 nematode isolates using LC-MS/MS and confirmed the presence of DNA 6mA
131 modification in 2 diploids (*M. graminicola* and *M. hapla*), 2 allotriploids (*M. incognita* and *M.*
132 *arenaria* 3n), and 2 allotetraploids (*M. arenaria* 4n and *M. javanica*) RKNs using SMRT-seq,
133 N6-Methyladenine DNA immunoprecipitation sequencing (6mA-DIP-seq), and DNA Dot blot
134 techniques. We discovered that 6mA primarily modifies active genes and found inconsistent
135 distribution landscapes of 6mA across different RKN species, especially in transposable
136 elements (TEs) between diploid and allopolyploid RKNs. Notably, low-methylation-level sites
137 in Mi were concentrated in the A2 subgenome, associated with genes involved in vital cell
138 functions, such as G protein-coupled receptors (GPCR). Importantly, we identified two putative
139 6mA demethylases (MiNMAD-1 and MiNMAD-2) and determined their catalytically active site
140 through structural prediction and biochemical experiments. Remarkably, host-induced gene
141 silencing of *minmad-1* significantly increased the resistance of transgenic host plants to 3
142 species of polyploid RKNs. Further study showed that the demethylase MiNMAD-1 globally
143 regulated the expression pattern of numerous virulence genes. Taken together, this work
144 establishes a link between eukaryotic pathogen epigenetics and virulence.
145

146 **Results**

147 **6mA widespread in nematode genome**

148 To investigate the status of DNA 6mA in nematodes, we collected 17 isolates of nematodes
149 including 7 RKNs, 4 isolates *Heterodera glycines*, 3 migratory plant-parasitic nematodes, 1
150 animal-parasitic nematodes, and 2 free-living nematodes. To exclude bacterial DNA
151 contamination during liquid chromatography coupled with tandem mass spectrometry
152 (LC-MS/MS) detection, we used sterile eggs from which DNA was extracted and used 16S
153 primers (27F, 1492R) to exclude the possibility of bacterial DNA contamination in the extracted
154 DNA (see Method, *SI Appendix*, Fig. S1). Finally, we found a distinct 6mA signal across all
155 species (Fig. 1*A*).
156
157 To further understand the role of 6mA methylation in the life history of PPNs, we focused on
158 several species of RKNs (*SI Appendix*, Tables S1 and 2). PacBio sequencing is widely used
159 for detecting 6mA modifications at single-base resolution; however, the issue of false positives
160 due to bacterial contamination is a significant concern. In this study, we employed the
161 6mASCOPE(34) approach to quantify bacterial contamination by aligning the PacBio sequel I

reads to the NCBI nt database. Our results showed that only 0.0004%-0.11% of reads originated from such contaminants (*SI Appendix*, Tables S3). To further assess the accuracy of these contamination ratios, we generated HiFi sequencing data for Mi, Ma, and Mj and analyzed them using 6mASCOPE. The results revealed that the proportions of reads originating from fungal and bacterial contamination were 0.018%, 0.011%, and 0.011% (*SI Appendix*, Tables S4-6), respectively. The results evaluated by 6mASCOPE support that the contamination rate in our data is extremely low. Subsequently, we analyzed the 6mA content of our previously constructed genome of *M. graminicola* (Mg), Mi, *M. arenaria* 3n (Ma 3n), *M. arenaria* 4n (Ma 4n), and *M. javanica*(44) by using PacBio sequel I data, and the results confirmed the LC-MS/MS data. In addition, we generated a chromosome-level genome assembly for the diploid *M. hapla* (Mh, *SI Appendix*, Tables S7) based on Pacbio, Illumina, and Hi-C data (*SI Appendix*, Tables S8). The genome size of this assembly closely matches with previous version(45) (53.1 Mb vs. 53.6 Mb), but shows a higher quality than previous version, as evidenced by an improved scaffold N50 (2.8 Mb vs. 0.08 Mb) and BUSCO 66.8%. We also identified the 6mA modifications at individual base level through PacBio sequel I data for Mh. To minimize false positives, we excluded 6mA sites with low sequencing coverage, using different minimum coverage thresholds (ranging from 15× to 50×) depending on the sequencing depth of each sample, as previously described(13, 17). After this filtering step, numerous 6mA sites were identified across the six genomes (*SI Appendix*, Tables S9). Subsequently, to further minimize false positives in 6mA analysis, we performed whole-genome amplification (WGA) on the genomic DNA of Mi, Ma, Mj, Mg, and Mh. To evaluate the reliability of 6mA site detection, we used WGA samples sequenced by PacBio HiFi as negative controls. The number of 6mA sites identified in these WGA samples, which should not contain true methylation, reflects the false-positive rate (*SI Appendix*, Tables S9 and S10). We observed that samples with minimal bacterial contamination—such as Ma 4n—had very few false-positive 6mA sites. In contrast, WGA samples with higher contamination levels yielded substantially more false-positive sites (*SI Appendix*, Tables S10 and S11). These findings highlight the importance of controlling for contamination when interpreting 6mA methylation data.

To further validate the presence of 6mA in RKNs genome, after excluding RNA m6A contamination (*SI Appendix*, Fig. S2, see **Method**), we conducted 6mA Dot blot on the egg genomic DNA of *M. incognita*, *M. arenaria* 3n, *M. arenaria* 4n, *M. javanica*, *M. graminicola*, and *M. hapla*, detecting a clear 6mA signal (Fig. 1*B*, *SI Appendix*, Fig. S3). However, no 6mA signal was detected in the negative control of nematode DNA after whole genome amplified (WGA) using phi29 polymerase (Fig. 1*B*) and 18S amplification (*SI Appendix*, Fig. S3). Next, we applied LC-MS/MS to distinguish 1mA from 6mA in these six genomic DNAs, with only 6mA signal being visible (Fig. 1*C*). Additionally, we performed 6mA-DIP-seq on Mi genomic DNA and Mi-WGA DNA (*SI Appendix*, Fig. S4*A*). Pearson correlation analysis confirmed high reproducibility between replicates (*SI Appendix*, Fig. S4*B*). The results verified the presence of 6mA in the Mi genome, with 53% of the peaks overlapping with those identified by SMRT sequencing (*SI Appendix*, Fig. S4*C*, *D*). However, only dozens of peaks were identified in the 6mA-DIP-seq data of Mi-WGA (*SI Appendix*, Tables S12). Taken together, all the results support the presence of 6mA in RKN genomes.

206

207 **6mA distribution landscape in nematodes genome**

208 The distribution of DNA methylation sites were found related to the expression regulation of
209 genes(46)**.** To comprehensively investigate regulatory effects of 6mA methylation on gene
210 expression in RKNs and free-living nematode *C. elegans* (Ce, download form GEO database,
211 GSE66504), we categorized all 6mA-modification-related genes based on their location at
212 promoter, gene body, and distal intergenic positions. We found the most 6mA sites in the gene
213 body and promoter, with the promoter region of Ce showing the highest proportion (59.93%) of
214 6mA distribution (Fig. 2*A*; *SI Appendix*, Fig. S5). Subsequently, we selectively extracted 6mA
215 sites distributed in the promoter, gene body, and distal intergenic regions, and focused on the
216 8-base-pair sequence surrounding each 6mA site for motif analysis. Within the same species,
217 the results indicate that the motifs of 6mA, whether located on the promoter, gene body, or
218 distal intergenic regions are generally similar (*SI Appendix*, Fig. S6). However, when
219 comparing those motifs between different species, there is a higher degree of conservation
220 among RKNs, whereas the motifs between RKNs and Ce show significant differences (*SI*
221 *Appendix*, Fig. S6). Additionally, the results demonstrated that the core motif in RKNs is GAG,
222 whereas in Ce it is ApT, consistent with findings in fungi. This suggests potential differences in
223 the patterns of 6mA-regulated gene expression between RKNs and Ce.

224

225 To investigate the functions of genes at different 6mA methylation levels, we classified the
226 6mA sites into 3 categories including low- (at a specific locus, less than 30% of reads in all
227 sequencing data are detected as methylated), moderate- (30%-70%) and high- (70%-100%)
228 methylation levels. We found that moderate-methylation-level 6mA sites exhibited the highest
229 density in Ce, Mi, Ma 3n, and Mj, accounting for about 76% in total 6mA sites. In Ma 4n, Mg,
230 and Mh, approximately 50% of the 6mA sites exhibited moderate-methylation-levels, while
231 only a small proportion showed either high or low methylation levels (Fig. 2*B*). Analyzing the 8
232 bp sequence surrounding 6mA sites revealed three distinct motifs across the methylation
233 categories in each nematode (Fig. 2*C*), respectively. The GAG motif was most represented in
234 6mA sites with high-methylation-level across the four RKNs (Mi, Mj, Mg, and Mh), similar with
235 findings in *C. elegans*(13) and rice(19, 20). In contrast, motifs at moderate and low methylation
236 levels varied among species (Fig. 2*C*), suggesting that different methylation levels of 6mA
237 sites may require diverse modifying enzymes and fulfill varied regulatory functions.

238

239 Subsequently, we examined the distribution density of 6mA in the gene regions and
240 transposable elements (TE) regions of these nematode genomes. The result shows that the
241 gene regions displayed a low distribution density of 6mA in all nematodes, except Mh (Fig. 2*D*),
242 which is similar to the 5mC distribution characteristics(19). TE regions showed significant
243 differences in the distribution density of 6mA sites among the polyploidy nematodes and the
244 diploid (Ce, Mg, and Mh) nematodes (Fig. 2*E*), indicating that 6mA and TE interactions might
245 relate to polyploid RKNs' characteristics post-polyploidization.

246

247 To investigate the distribution patterns of 6mA in TE regions in polyploid and diploid
248 nematodes, we scrutinized the abundance of 6mA across various types of TE in both polyploid
249 and diploid nematodes. We found that 6mA in polyploid nematodes is densely distributed in

250 DNA TE, MITE, and LTR, with a low density in the Low_complexity region, which has a
251 low-density feature like the gene region (*SI Appendix*, Fig. S7-10). We noticed that the TE
252 content and type between polyploid and diploid RKNs are significantly difference (*SI Appendix*,
253 Tables S13). About 28%-33% of the genome sequences in polyploid RKNs are TE, of which
254 8%-10% types of TE are Low_complexity TE (including simple repeat). While in diploid RKNs,
255 only 8%-10% of the genome is comprised of TE, and 41%-81% of those TE are low complexity.
256 However, the differences in TE types cannot explain the significant difference in the
257 abundance of 6mA in polyploid and diploid nematodes' TE regions, even though diploid
258 nematodes contain a high proportion of DNA TE, MITE-type TEs still do not have the
259 high-density 6mA feature in these regions (*SI Appendix*, Fig. S11-13). For example, *C.*
260 *elegans* has the similar distribution of TE types as polyploid RKN (*SI Appendix*, Tables S13),
261 but the distribution of 6mA on TE exhibits the same characteristics as diploid nematodes. To
262 verify the authenticity of our data, we performed the same analysis on the false-positive 6mA
263 sites predicted in the WGA sample sequencing data. The results showed that these
264 false-positive 6mA sites did not have an increased density in the TE region, nor a decreased
265 density in the gene region (*SI Appendix*, Fig. S14), but were randomly distributed in the
266 genome. To further verify the authenticity of 6mA enrichment at TE positions, we compared
267 the overlap ratio of 6mA-DIP-seq peaks with the TE regions of Mi. We found that 74.8% of the
268 merged peaks identified by 6mA-DIP-seq overlapped with the TE region of *M. incognita*, while
269 Mi's TE region only accounted for 28.18% of the total genome. These results indicate that the
270 high-density 6mA feature of TEs in polyploid RKNs is not related to TE type and may be
271 related to TE outbreaks and maintenance of genome stability after polyploidization.
272
273 **6mA regulates gene expression of RKNs**
274 To understand the impact of 6mA methylation on gene expression levels, we examined the
275 relationship between 6mA methylation and gene expression from multiple aspects. Firstly, we
276 compared the expression levels in egg stage (same stage as collecting SMRT sequencing
277 data) of 6mA-methylated genes and unmethylated genes in these six RKNs. The results
278 suggested that the expression levels of 6mA-methylated genes in almost all the RKNs were
279 significantly higher than those of unmethylated genes, while the opposite pattern was
280 observed in Mh (Fig. 3*A*). Among all polyploid RKNs, genes with an unmethylated status
281 predominantly exhibit a low expression level, measured by transcripts per million (TPM)<1.
282 Conversely, within methylated genes, there is a higher proportion showing an expression level
283 exceeding TPM>5 (Fig. 3*B*). In diploid RKNs, regardless of methylation status, most genes
284 demonstrate an expression level surpassing TPM>5. Conversely, in the free-living nematode
285 Ce, the predominant proportion of genes exhibit TPM<1 (Fig. 3*B*). These findings suggest that
286 genes modified by 6mA methylation tend to activate gene expression in polyploid species,
287 while no significant trend is observed in diploid nematodes.
288
289 Subsequently, to investigate whether there are differences in modification site motifs among
290 genes with different expression levels of genes modified by 6mA, we performed motif
291 enrichment analysis on the 6mA sites of genes (egg stage) with TPM<1, 1<TPM<5, and
292 TPM>5, respectively. The results indicate that genes with different expression levels within the
293 same species exhibit similar motif enrichment, and motifs among RKNs are relatively

294 conserved, with a core motif of GAG (*SI Appendix*, Fig. S15). In contrast, there is a significant
295 divergence in motifs between Ce and RKNs, with the core motif being ApT (*SI Appendix*, Fig.
296 S15). Notably, the motif patterns associated with genes of different expression levels are
297 similar to those observed for 6mA sites located in different genomic regions, such as
298 promoters, gene bodies, and distal intergenic regions (*SI Appendix*, Fig. S6).
299
300 Secondly, many previous studies have shown that differences in DNA methylation modification
301 sites (promoter, gene body, and distal intergenic regions) are often related to gene expression
302 regulation. Hence, we extracted the genes modified at one of these three positions alone and
303 simultaneously modified at three modification positions (*SI Appendix*, Fig. S16) to explore the
304 expression differences between genes modified at these different positions. The analysis of
305 gene expression levels revealed that genes modified by 6mA in the gene body position in
306 polyploid RKNs (Mi, Ma 3n, Ma 4n, and Mj) exhibited higher expression levels than the overall
307 average of all genes (Fig. 3*C*). While the genes modified by 6mA at promoter in diploid RKNs
308 presented a higher expression level than the overall average of all genes (Fig. 3*C*). Besides,
309 the expression levels of promoter-methylated genes and gene body-methylated genes in Ce
310 are both higher than the overall average of all genes (*SI Appendix*, Fig. S17), which is different
311 from the characteristics of RKNs. These results indicate that 6mA regulates gene expressions
312 differently in polyploid and diploid RKNs.
313
314 Thirdly, to explore the impact of methylation levels on gene expression regulation, we
315 investigated the expression levels of the genes at different 6mA methylation levels (low-,
316 moderate- and high-methylation levels). The results show that in Mi, Ma 3n, and Mg the
317 moderate-methylation-level related genes exhibited the highest expression level, while in Ce
318 and Mh, the high-methylation-level related genes displayed the highest one (Fig. 3*D*),
319 suggesting that the effect of 6mA on gene expression levels is a divergence in different
320 nematodes.
321
322 Finally, we compared the expression levels of the transposable element-related genes (TEGs)
323 and 6mA-marked genes, as previously described(19). Interestingly, the genes unmodified by
324 6mA and TE displayed the lowest expression level in all six nematodes except Mh, and the
325 triploid RKNs (Mi and Ma 3n) have a similar expression signature, while diploid and tetraploid
326 RKNs do not (Fig. 3*E*). Further, we compared the TPM of 6mA-modified genes with and
327 without TE nearby and found the 6mA-modified genes with no TE nearby displayed a lower
328 expression level than those with TE nearby in Ma 3n, Ma 4n, Mj, Mg, and Ce, which was the
329 opposite in Mi and Mh (*SI Appendix*, Fig. S18). However, the 6mA-marked TEGs showed
330 significantly higher expression levels than the 6mA-unmarked ones in all nematodes (*SI*
331 *Appendix*, Fig. S18). These findings suggest that although 6mA is frequently enriched in
332 TE-rich genomic regions, its influence on gene expression differs depending on genomic
333 context and nematode lineage. This indicates that the regulatory role of 6mA is multifaceted,
334 functioning neither as strictly repressive nor exclusively activating, but instead showing
335 context-dependent associations with gene expression.
336
337 **Low-methylation-level 6mA sites play a crucial role in Mi**

338 In addition, we examined the abundance of 6mA on each chromosome in these six RKNs.
339 Notably, the distribution of 6mA was different on some chromosomes of Mi, Ma 3n, and Ma 4n,
340 but evenly distributed on the chromosomes of Mj, Mg and Mh (*SI Appendix*, Fig. S19). Overall,
341 A_2 subgenome showed a higher 6mA content in Mi genome. Additionally, the mitochondria
342 DNA in all six RKNs presented the highest 6mA abundance (*SI Appendix*, Fig. S19), which
343 was similar to that in human(22). Recent study has revealed that 6mA on *C. elegans*
344 mitochondria DNA responds to environmental stress(29, 47). We speculate that 6mA in RKNs
345 might be involved in their response to stress from host plants.
346
347 Subsequently, we investigated the distribution status of 6mA sites with different methylation
348 levels on the RKNs genome and plotted the data by Circos (*SI Appendix*, Fig. S20*A*). We
349 noticed that the three methylation-level 6mA sites presented an even distribution on the
350 chromosome of these six RKNs, except for the low-methylation-level 6mA sites in Mi (*SI*
351 *Appendix*, Fig. S20*A*, green circle of Mi). We found that 72% of the high-density-region (HDR,
352 6mA counting beyond 60 in a 50 kb genome window) of low-methylation-level 6mA sites were
353 in the A_2 subgenome. Further, we extracted the genes related to the HDR of low-methylation
354 sites from A_2 subgenome, and the genes located in the same region from A_1, and B_1
355 subgenomes to compare their expression level in egg stage. Notably, the genes from A_2
356 subgenome presented a higher expression level than those from A_1 and B_1 subgenomes (*SI*
357 *Appendix*, Fig. S21). Furthermore, these genes showed the higher expression level not only in
358 the egg stage (the stage we collected the information of 6mA sites) of Mi, but also in the other
359 stages of Mi (*SI Appendix*, Fig. S20*B*).
360
361 To reveal functional differences of the genes related to the HDR of low-methylation-level 6mA
362 sites between A_2 and A_1 or B_1 subgenome, we compared the enriched Pfam structure domain
363 of these genes. The results showed that the genes from A_2 subgenome were enriched in
364 GPCR (*SI Appendix*, Fig. S20*C*), which were consistent with the GO enrichment analysis
365 results of the genes with high methylation density in human(22). GPCR superfamily is one of
366 the larger chemoreceptors, and it acts as a center receptor in nematodes which will become
367 "blind" and "deaf" without GPCR(48). GPCR also plays an important role in fungal infection(49,
368 50), and it may play an extremely important role in finding hosts and secreting effectors for
369 RKNs(51). Moreover, we performed the GO analysis of these related genes in A_2, A_1, and B_1
370 subgenomes. The results showed that these genes from A_2 subgenome were mainly enriched
371 in important molecule function GO terms such as pharyngeal gland morphogenesis in Mi (*SI*
372 *Appendix*, Fig. S20*D*). These results suggested that the genes modified by
373 low-methylation-level 6mA sites from A_2 subgenome were involved in many important
374 biological processes in Mi, and these genes played a more important role in A_2 subgenome
375 than in A_1 and B_1 subgenomes.
376
377 **MiNMAD-1/2 are involved in 6mA demethylation**
378 A previous study identified three 6mA methyltransferases from Mi, while the 6mA demethylase
379 remained unidentified(43). To verify whether Mi has 6mA demethylase, we synthesized an
380 oligo DNA with 6mA and biotin labeling and uncovered its 6mA level after treating oligo DNA
381 with broken Mi eggs suspension. Compared with the broken egg suspension after heat

treatment control, and BSA control, the 6mA content in the treatment group was significantly reduced (*SI Appendix*, Fig. S22a), suggesting that there are one or more potential 6mA demethylases in Mi.

We collected 6 genes containing 2OG-FeII_Oxy_2 domain based on Pfam annotation and 3 genes with the highest sequence similarity to demethylase gene *nmad-1* of *C. elegans* from our newly assembled Mi genome to identify the putative demethylase genes in Mi. The phylogenetic tree showed that these 9 putative demethylase genes (three alleles) belonged to *alkbh1*, *alkbh6,* and *alkbh7* family in Mi, Ma 4n, Mj, Mg, and Mh (Fig. 4*A*; *SI Appendix*, Fig. S23). To investigate whether these genes had functions of 6mA demethylases, we detected genomic DNA 6mA level after RNAi of these genes in Mi eggs by LC-MS/MS. The results showed that *Mi_14752.1* and *Mi_00010.1* knock-down significantly increased 6mA level, while *Mi_23849.1* knock-down did not (Fig. 4*B*; SI Appendix, Fig. S22*B*).

We purified these three proteins and tested their demethylation activity *in vitro* and found that both Mi_14752.1 and Mi_00010.1 demethylated genomic DNA in Mi (Fig. 4*C*, *D*; *Supplemental* Fig. S24). To further examine the 6mA demethylation activity of these two proteins, we used the oligo DNA with 6mA modification and treated it with these three proteins *in vitro* and observed a significant demethylase activity in Mi_14752.1 and Mi_00010.1 (Fig. 4*E*). Furthermore, we comparatively analyzed the sequence similarity between these two proteins and the reported demethylases. We found that although the demethylases in these different species have large sequence divergence, their catalytic active sites are highly conserved (*SI Appendix*, Fig. S25*A*). We predicted the 3D structure of Mi_14752.1, Mi_00010.1, Mi_23849.1, and Ce_NMAD-1 by using Alphafold2(52). The results show that Mi_14752.1 is highly like human ALKBH7 in structure, showing root-mean-square deviations (RMSD) of 0.067 Å (*SI Appendix*, Fig. S25*B*). In addition, the catalytic sites of Ce_NMAD-1 overlaps with the sites of Mi_14752.1 and Mi_00010.1 in 3D structure (*SI Appendix*, Fig. S25*C*, *D*) but does not overlap with the Mi_23849.1 sites (*SI Appendix*, Fig. S25*E*). Besides, the RMSD between Ce_NMAD-1 and Mi_14752.1, Mi_00010.1, and Mi_23849.1 are 2.392, 1.066, and 12.625 Å, respectively (SI Appendix, Fig. S25*C*-*E*). To further elucidate whether the demethylating activity is intrinsic to Mi_14752.1 and Mi_00010.1, we introduced mutations (H153A and D155A for Mi_14752.1, and H104A and D106A for Mi_00010.1). Subsequently, we observed that these mutations led to the abolition of their demethylation activity (Fig. 4*F*). Thus, we designated Mi_14752.1 as Mi N6-methyl adenine demethylase 1 (MiNMAD-1) and Mi_00010.1 as MiNMAD-2 to reflect their newly found demethylation functions.

Host-induced gene silencing (HIGS) of *minmad-1*/*2* reduces infectivity of Mi

Considering most stages of RKN life cycle are in plants, we constructed transgenic tobacco expressing *minmad-1*/*2, Mi_23849.1* (verify whether it has demethylase activity during the Mi infection period), and *gfp* dsRNA to study the regulation functions of 6mA in parasitic stage of Mi. Three-week pot experiments showed that compared to *gfp*-HIGS and CK tobacco, *minmad-1*/*2*-HIGS tobacco plants exhibited different resistances to Mi, while *Mi_23849.1*-HIGS tobacco shows no significant difference (Fig. 5*A*). The eight-week pot experiment showed that the galls number was dropped by 10 folds in high-expression line of

426 *minmad-1/2*-HIGS tobacco, compared to those in *gfp*-HIGS and CK tobacco (Fig. 5*B*; *SI*
427 *Appendix*, Fig. S26*A*, *B*). As expected, compared with that of control, the 6mA level of Mi
428 genomic DNA after infesting the *minmad-1/2*-HIGS tobacco displayed a significant increase
429 (Fig. 5*C*), confirming that MiNMAD-1/2 were the demethylases in Mi. Subsequently, according
430 to galls number, we divided the nematode-infested *minmad-1*/*2*-, and *Mi_23849.1*-HIGS
431 tobacco plants into three groups including multiple-, medium-, low-galls groups (*SI Appendix*,
432 Fig. S27*A*-*C*). After confirming that bacterial contamination has been eliminated (see Method),
433 the DNA of females and eggs was extracted from the three groups for 6mA level detection.
434 The results showed that the 6mA content was negatively correlated with galls number (Fig.
435 5*D*), indicating that demethylase silencing reduce virulence of Mi. Additionally, the 6mA level
436 of females was much higher than that of eggs (Fig. 5*D*), indicating a stage-specific difference
437 in 6mA levels during development. To further explore the RKNs resistance effect of
438 demethylase gene in different plants, we constructed *minmad-1*-HIGS tomato. The tomato pot
439 experiments also showed that RNAi with demethylase increased resistance of hosts to Mi (*SI*
440 *Appendix*, Fig. S28*A*-*C*), and the level of 6mA in Mi after fed on transgenic tomato increased
441 significantly (*SI Appendix*, Fig. S28*D*). These results suggest the feasibility of transgenic plants
442 expressing Mi demethylase dsRNA to confer Mi resistance in plants.
443
444 Additionally, the sequences of *minmad-1* are completely conserved among polyploid RKNs (*SI*
445 *Appendix*, Fig. S29), suggests that the transgenic plants expressing Mi demethylase gene
446 dsRNA may confer resistance to multiple polyploid RKNs. To verify this conjecture, we carried
447 out an experiment of measuring the pot infection ability of transgenic tobacco to other polyploid
448 RKNs. The results showed that the *minmad-1*-HIGS tobacco plants exhibited significant
449 resistance to tetraploid RKNs Mj and Ma 4n compared to the CK and *gfp*-HIGS control plants
450 (Fig. 5*E*, *F*; *SI Appendix*, Fig. S30*A*, *B*). In addition, the 6mA level of Mj and Ma 4n genomic
451 DNA was significantly increased in *minmad-1*-HIGS group (Fig. 5*G*, *H*). Finally, to examine the
452 role of demethylases in diploid RKN, we constructed transgenic rice expressing Mg putative
453 demethylase dsRNA. However, the result shows that transgenic rice has no resistance to Mg,
454 even though 6mA levels were significantly elevated in nematodes fed transgenic rice (*SI*
455 *Appendix*, Fig. S30*C*-*F*). These results suggest that demethylase may influence the virulence
456 of RKNs, but demethylases may have distinct effects on RKNs of varying ploidies.
457
458 **6mA regulates the expression pattern of the Mi virulence gene effector**
459 To further investigate the regulatory effect of 6mA demethylase on Mi, we grew 80
460 *minmad-1*-HIGS tobacco plants inoculated with Mi. According to the infestation by Mi, we
461 divided the 80 tobacco plants into 8 groups namely, 1-2 groups with multiple galls (less than
462 the gall number of control), 3-6 groups with medium galls, and 7-8 groups with few galls, and
463 then we collected the infestation J3J4 larvae from these 3 groups for RNA-seq (*SI Appendix*,
464 Tables S14). A total of 7198, 8978, and 8660 DEGs were obtained (*SI Appendix*, Fig. S31)
465 from multiple-, medium-, low-galls groups, respectively. The 4667 DEGs were shared by all
466 three galls groups (*SI Appendix*, Fig. S32*A*) and displayed two significantly different
467 expression patterns (*SI Appendix*, Fig. S32*B*). The number of DEGs unique to one of three gall
468 groups (multiple-, medium-, low-galls) was 832, 1685, and 1491, respectively (*SI Appendix*,
469 Fig. S32*A*). Functional analysis of DEGs showed that numerous enriched down-regulated

470 DEGs unique to medium galls group were ribosome genes (*SI Appendix*, Fig. S32*C*),
471 suggesting that demethylase might regulate ribosomal level, thus modulating the translation
472 efficiency of mRNA, ultimately reducing Mi infectivity.
473
474 To explore the major cause of the reduced infectivity of Mi in *minmad-1*-HIGS tobacco plants,
475 we examined Mi's virulence gene (effectors), which represent its most important weapons for
476 parasitizing the host. We compared the putative secreted proteins (including effectors, amount
477 to 2,324) from 4667 shared genes, and 520 secreted proteins have been screened (*SI*
478 *Appendix*, Fig. S32*A*). The secreted proteins in all the three gall groups had a lower
479 expression level than those in the control group (*SI Appendix*, Fig. S32*D*), and the few galls
480 group displayed the lowest expression level among three gall groups (*SI Appendix*, Fig. S32*E*),
481 indicating that the Mi resistance of transgenic plants was negatively correlated with the
482 expression of Mi effector.
483
484 Nematode invasion into plants requires many processes such as chemotaxis, host
485 identification, cell wall degradation, establishment and maintenance of feeding sites, and
486 defense against plant immunity(53). Different processes require different effectors, and the
487 correct expression patterns of effectors are essential for host infestation. The expression
488 profiles showed that all the putative secreted protein genes from control groups and RNAi
489 groups fell into 11 clusters, the RNAi group displayed an expression pattern completely
490 opposite to control group (Fig. 6*A*). These results indicated that demethylase might affect the
491 expression pattern of Mi effector globally, thereby regulating the ability of Mi to infest plants.
492
493 To further investigate the regulation effect of demethylase on the effector, we compared the
494 expression levels of some reported effectors of the nematodes from *minmad-1*-HIGS tobacco
495 and *gfp*-HIGS control tobacco by qRT-PCR. The results showed that compared with those in
496 *gfp*-HIGS control, effectors Mi-XYl1, Mi-CRT, Mi8D05, MiPFN3, 16D10, MiSGCR1, and
497 MiIDL1 were down-regulated 22, 126, 10, 28, 27, 5 and 13 folds in females, respectively (Fig.
498 6*B*; *SI Appendix*, Fig. S33; *SI Appendix*, Tables S15). To determine whether the effector
499 exhibited the same decrease at protein level, we prepared the antibody of Mi-CRT. Western
500 blot assay showed that *minmad-1* RNAi significantly reduced the protein accumulation of the
501 effector Mi-CRT compared to the gfp-HIGS and CK controls (Fig. 6*C*). In addition, Mi-CRT
502 expression was down-regulated in both the female and egg stages (Fig. 6*D*), suggesting that
503 6mA DNA methylation may affect effector expression, likely at the transcriptional level, which
504 in turn leads to reduced protein levels.
505
506 To determine whether the demethylase directly binds to and regulates polyploid RKNs
507 effectors, we generated a specific antibody against the enzyme and performed ChIP-seq
508 analysis on infective J2s (*SI Appendix*, Fig. S34*A*), the only stage capable of host invasion.
509 The results revealed that 40.4%–51.7% of the candidate effector genes were bound by the
510 demethylase (*SI Appendix*, Fig. S34*B-D*). We next performed 6mA-DIP-seq on Mi J2s to
511 further assess whether 6mA directly marks the candidate effector genes. Approximately 40%
512 of the candidate effector genes carried 6mA modifications, and notably, 47.4% of these
513 overlapped with demethylase ChIP-seq targets (*SI Appendix*, Fig. S35). Together, these

514 findings demonstrate that the enzyme directly acts on effector genes and may influence their
515 transcriptional regulation.
516
517 Based on the above results, we speculate that the 6mA regulatory mechanism at the
518 molecular level may be that 6mA methyltransferase and demethylase dynamically regulate the
519 6mA methylation level of effector in a spatiotemporal specific manner, thereby affecting its
520 expression level at different stages (Fig. 6*E*). Our data suggested that epigenetic regulation
521 could be one of the major factors responsible for the parasitic ability of RKNs by regulating the
522 expression pattern of virulence effectors. Whether 6mA regulates transcription factors in this
523 process and thus more broadly regulates the expression of effectors is worthy of further study.
524
525 **Discussion**
526 In recent years, there has been considerable controversy regarding 6mA modification in
527 eukaryotes, mainly regarding the issue of bacterial DNA contamination. Considering these
528 concerns, we eliminated the possibility of false positives through multiple methods. (i) Our
529 sample of Fig. 1 were collected from axenic eggs after parasitizing axenic cultures of tobacco;
530 (ii) Tissues extracted from all DNA samples (egg, J3J4, female) we tested for 6mA were
531 passed through sodium hypochlorite to eliminate potential surface bacteria before being
532 ground and plated on LB and PDA media to confirm the absence of commensal bacteria; (iii)
533 We performed 16S amplification on the extracted nematode DNA and found no amplified
534 bands of bacterial DNA; (iv) The SMRT-seq data were first aligned to the nematode genome,
535 and reads with a coverage of at least more than 15× were screened out before being used to
536 call 6mA sites, further eliminating the possibility that the signal came from bacterial
537 contamination DNA. (v) We removed potential false-positive 6mA sites from our data by
538 sequencing and analyzing WGA samples using PacBio and 6mA-DIP-seq. (vi) We used
539 6mASCOPE to assess the proportion of bacterial/fungal contamination in HiFi sequencing
540 data, which was only about 0.01%. (vii) We confirmed the exclusion of RNA m6A
541 contamination in DNA by LC-MS/MS (DNA 6mA: 266.1>150.0; RNA m6A: 282.1>150.0).
542 However, the assessment of 6mA levels in other migratory parasitic nematodes, especially
543 those that feed on both fungi and plants, and free-living nematodes that feed on bacteria,
544 should be more cautious. We believe that the egg stage (the most stage used in this study)
545 should be the period with the least bacterial contamination, because there is no intestinal
546 tissue, which reduces the possibility of symbiotic bacteria. In addition, our WGA HiFi data
547 show that the higher the proportion of bacterial contamination in the sample, the higher the
548 proportion of false positive 6mA identified by ipdSummary, which is one of the reasons why
549 many 6mA in many eukaryotic organisms have been proven to be erroneous (34). Our data
550 has been verified to show that the contamination ratio is as low as 0.01%, so the credibility of
551 the results is relatively high.
552
553 Methylation is an epigenetic modification of the genome that can affect gene expression and
554 genome stability. The high density of 6mA methylated sites in TE regions may have an impact
555 on their stability and expression, thereby affecting their function. In addition, highly methylated
556 TE regions may also have an impact on the structure and compactness of chromatin, thereby
557 affecting the three-dimensional structure of the genome and the accessibility of chromosomes.

558 TE regions often have highly repetitive sequences that may be prone to recombination and
559 insertion, leading to genomic instability and mutation(54). However, methylation of 6mA may
560 contribute to the stability of TE regions, thereby reducing the occurrence of these structural
561 changes. In addition, the high-density 6mA methylated TE region may help to maintain this
562 important genetic information and play an important role in the evolution and adaptability of
563 species. Interestingly, the high density of methylation in the TE region is considered to be
564 related to the reduced expression of TE neighboring genes (TEGs)(55), while our results found
565 that the expression level of TEGs with 6mA methylation was significantly higher than those
566 without methylation.
567
568 Our results reveal that transposable element (TE) regions in polyploid nematodes exhibit
569 high-density 6mA methylation, whereas diploid nematodes lack such enrichment. Given that
570 TEs are often associated with phenotypic diversity, stress responses (56), a comparative
571 analysis of 6mA distribution patterns between polyploid and diploid RKNs is warranted to
572 better understand the mechanistic basis underlying these differences. Additionally, examining
573 the relationship between infection ability and 6mA among RKNs of different ploidy may provide
574 further insights into the biological implications of 6mA. While we observed distinct genomic
575 and transcriptomic features between polyploid and diploid RKNs, we acknowledge that these
576 differences may not solely result from polyploidy. Notably, polyploid RKNs included in this
577 study are also more closely related to each other phylogenetically, which raises the possibility
578 that some of the observed features reflect shared evolutionary history rather than ploidy
579 effects per se. Disentangling the influence of polyploidy from lineage-specific adaptations will
580 require broader sampling of RKN species, including both closely and distantly related diploid
581 and polyploid taxa. Future studies incorporating independent polyploidization events and more
582 resolved phylogenies will be critical to clarify the relative contributions of genome duplication
583 and phylogenetic proximity to the traits observed.
584
585 The AlkB family, as dealkylating enzymes, is conserved from bacteria to humans(57, 58), and
586 there are 9 AlkB proteins in humans (AlkB1-8 and FTO), of which ALKBH1 and ALKBH4 are
587 mostly confirmed to have demethylase function. ALKBH1 has been demonstrated to be a
588 demethylase in human(22), mouse(59), and rice(19), while demethylase NMAD-1 in *C.*
589 *elegans* is a homologue of ALKBH4(13). In this study, we have identified three proteins
590 containing 2OG-FeII_Oxy_2 domain from Mi. Our *in vivo* and *in vitro* assays suggested that
591 two proteins homologous to ALKBH6 and ALKBH7 function as putative 6mA demethylases in
592 triploid Mi. Furthermore, we observed that sequences with varying methylation levels
593 corresponded to distinct motifs, and these motifs may correspond to different modifying
594 enzyme systems.
595
596 Finally, our data suggest that 6mA can directly affect the expression of nematode virulence
597 genes, but we believe that 6mA is also likely to regulate virulence indirectly by modulating the
598 expression of key transcription factors. In addition to these effects, it is important to note that
599 6mA methylation is a genome-wide epigenetic mark, and its influence on nematode biology is
600 not confined to virulence gene regulation. Rather, 6mA might contributes broadly to essential
601 physiological processes, including development, reproduction, and stress responses,

602 consistent with its role in shaping chromatin accessibility and transcriptional dynamics across
603 the genome. Besides, the *minmad-1*-HIGS of tomato and tobacco significantly enhanced the
604 resistance of transgenic plants to polyploid RKNs (Mi, Ma, and Mj), while rice with
605 Mg-demethylase HIGS had no significant effect on Mg infection, and knockout the
606 demethylase of *C. elegans* only slightly decreased average egg-laying rate(13). The functional
607 differentiation of demethylase between polyploid and diploid nematodes might be because
608 epigenetic regulation played a more important role in parthenogenetic organisms than in
609 sexually reproducing organisms. Further work of 6mA analysis in more parthenogenetic and
610 sexual propagation RKNs might provide more insights into the role of 6mA in different
611 reproductive modes and different ploidy species. In summary, the connection between
612 pathogen virulence and epigenetics has been established, in-depth biological function
613 research on 6mA may screen many target resources for the control of RKNs and might provide
614 new perspectives and methods for the prevention and control of other agricultural pathogens.
615

616 **Materials and Methods**
617
618 **Nematode materials**
619 Our previously work has constructed the telomere-to-telomere *Meloidogyne incognita* WHF4-1,
620 *Meloidogyne arenria* SYMaF1-2, and *Meloidogyne javanica* LongYF2-1 genome,
621 chromosome-level *M. graminicola* (Mg) genome, and *M. hapla* (Mh) genome assembled in this
622 study were used for further 6mA DNA methylation studies. The nematodes were inoculated to
623 Rutgers tomato in greenhouse, 25 degrees centigrade, after 6 weeks of culture, the eggs, J3J4,
624 and female were collected for subsequent experiments. The DNA for SMRT-seq, LC-MS/MS
625 and Dot blot experiments came from the sterilized J2 nematodes inoculated into aseptically
626 cultured tobacco in MS medium (plant gel instead of agar powder). After 35 days, the sterile
627 eggs were collected for the subsequent experiment. The nematode native DNA and WGA
628 DNA used for HiFi sequencing and Mi-WGA 6mA-DIP-seq were collected from nematode eggs
629 after infecting potted host plants. Before DNA extraction, the eggs were disinfected with 10%
630 sodium hypochlorite to minimize bacterial contamination.
631
632 **Nematode collection**
633 Three stages of RKNs were used in this study. For egg collection, cut the nematode-infected
634 tomato or tobacco roots into 0.5 cm size, put it into a 500 ml beaker, followed by adding 225 ml
635 ddH2O and 25 ml sodium hypochlorite, and place it on a magnetic stirrer for 8 minutes at 1000
636 rpm. The suspension was successively passed through 18, 60, 100, 200 and 500 mesh sieves,
637 rinsed five times with water to remove sodium hypochlorite, and the eggs were retained on the
638 500-mesh sieve. After sucrose gradient centrifugation with a final concentration of 35%, the
639 sucrose was passed through a 3um filter membrane using a negative pressure suction filter,
640 and the eggs retained on the 3 μm filter membrane were collected for the next experiment. For
641 J1 collection, the purified eggs were incubated for 2-3 days at 20 °C, J1 larvae were manually
642 picked out under a microscope until most of the eggs became intertwined worms. For J2
643 collection, the purified eggs were incubated on a 500-mesh sieve with water for 3-5 days at
644 20 °C, and the J2 larvae were collected from the water under the mesh. For J3J4 and female
645 collection, the roots after treated with sodium hypochlorite to collect the egg were put into a
646 mortar, then use a pestle to smash the roots lightly, suspend the roots with 100 ml of water,
647 and pass them through 18, 60, 100, and 200 mesh sieves in sequence. The J3J4 were on the
648 200 mesh sieves, and the female were on the 60 mesh sieves. After most plant debris was
649 removed by sucrose centrifugation, J3J4 were manually picked under a microscope, and the
650 females were picked visually. For early female (eFemale) collection, the tobacco roots 21 days
651 after nematode infestation were collected, and early females before oviposition were manually
652 picked out with forceps.
653
654 **Nematode gDNA Extraction**
655 Genomic DNA was extracted from eggs of RKNs and cyst nematodes, as well as from
656 mixed-stage individuals of *D. destructor*, *A. avenae*, *B. xylophilus*, *H. contortus*, *C. elegans*,
657 and *C. nigoni* for subsequent experiments. Before DNA extraction, sodium hypochlorite was
658 used to sterilize the nematodes and pass through a 3 μm filter to remove contamination such
659 as bacteria. Genomic DNA was isolated using the CTAB method as follow: (1) eggs were

660 suspended in 200 μl SDS-EB lysis buffer (50 mM Tris-HCl pH 8.0, 200 mM NaCl, 20 mM
661 EDTA, 2% SDS, 1mg/ml proteinase K) and transfer into liquid nitrogen; (2) after homogenized,
662 the powder was collected into 1.5 ml tube and add SDS-EB lysis buffer to 500 μl; (3) add 500
663 μl 65 °C preheat CTAB buffer (100 mM Tris-HCl pH 8.0, 20 mM EDTA, 1.4 M NaCl, 2% CTAB,
664 1% PVP 40000) and incubation at 65°C for 30 min; (4) equal volume
665 phenol-chloroform-isoamyl alcohol mix (25:24:1) were added to separate the DNA and protein,
666 mixture were spun at 13,000 rpm at 4 °C for 15 min, collect the supernatant; (5) 2 μl 10 mg/ml
667 RNase A was added into the supernatant and incubated at 37 °C for 15 min; (6) 0.75 M final
668 concentration ammonium acetate was added and DNA was sedimented in pre-cold
669 isopropanol (0.9:1, v/v) and finally dissolution in 30 to 50 μl DNase-free water.
670
671 **Eliminate bacterial DNA contamination and RNA m6A contamination**
672 To ensure the accuracy of 6mA detection in nematode DNA, we took several steps to
673 eliminate potential contamination from bacterial DNA and RNA-derived m6A. For initial tests,
674 all nematode genomic DNA was extracted from eggs. In the case of root-knot nematodes,
675 eggs were collected from parasitized roots grown under sterile tobacco culture conditions. To
676 minimize the possibility of bacterial contamination on the egg surface, eggs were disinfected
677 with sodium hypochlorite, followed by grinding and plating on LB and PDA media to test for the
678 presence of cultivable endophytes. Additionally, PCR amplification using universal 16S rRNA
679 primers (27F and 1492R) was performed on extracted DNA to screen for bacterial DNA.
680
681 To exclude RNA contamination in downstream 6mA detection methods such as dot blot and
682 6mA-IP-seq, RNase A treatment was applied to genomic DNA after extraction. RNA fragment
683 size was monitored to ensure efficient digestion, with fragments reduced to less than 100 bp.
684 DNA was then sonicated and size-selected using magnetic beads to retain fragments larger
685 than 200 bp. Liquid chromatography–tandem mass spectrometry (LC-MS/MS) was
686 subsequently used to differentiate between DNA-derived 6mA (molecular mass 266.1 > 150.0)
687 and RNA-derived m6A (282.1 > 150.0), allowing for confirmation that only 6mA signals
688 originated from DNA.
689
690 **6mA-DIP-seq and analysis**
691 The 6mA-DIP-seq was performed following the published protocols. Briefly, we fragmented 7
692 ug WHF4-1 RNA removed gDNA to 200-400 bp. After end repaired and adapter ligation by
693 using Vazyme ND607 VAHTS Universal DNA Library Prep Kit for Illumina V3, DNA was
694 heat-denatured and immunoprecipitated overnight at 4 °C with anti-6mA antibodies purchased
695 from Abcam (ab151-230). Input and 6mA immunoprecipitated DNA was PCR amplified using
696 Vazyme ND607 to construction the next generation sequencing library. The raw data were
697 filtered by using Cutadapt (v3.3)(60) and aligned to WHF4-1 genome by using bowtie2
698 (v2.3.0)(61). The low quality and duplicate reads were removed by using SAMtools (v1.7)(62)
699 and Picard (https://broadinstitute.github.io/picard/). Then, macs2 (v2.1.1)(63) was introduced
700 to give the enriched regions to call 6mA peaks by comparing the reads between 6mA-IP and
701 Input sample, with the following options: -B -SPMR -nomodel. The post file was further
702 transformed into bigwig format for the profile visualization by using deeptools (v3.5.1)(64) and
703 IGV (v2.5.2)(65). The MEME-ChIP(66) (https://meme-suite.org/meme/tools/meme-chip) was

704 used to identify the conserved motifs enriched in 6mA peaks.
705
706 **DNA/RNA library construction and sequencing**
707 Approximately 100 μl eggs were purified and collected for DNA extraction, and the genomic
708 DNA was isolated using the CTAB method as described in previously. The DNA was sent to
709 the ANNOROAD Gene Technology Co., Ltd. (Beijing, China) for PacBio library construction
710 followed by sequel I platform sequencing. RNA extracting was using the TransZol Up Plus
711 RNA Kit (TransGen Biotech, Beijinng, China) and RNA Nano 6000 Assay Kit of the
712 Bioanalyzer 2100 system (Agilent Technologies, CA, USA) was using to assess the RNA
713 integrity and concentration. The RNA library preparation was followed the protocol of VAHTS®
714 Universal V8 RNA-seq Library Prep Kit for Illumina (Vazyme, Nanjing, China). Finally, the
715 library was pooled and sequenced on Illunima NovaSeq platform with 150 bp paired-end reads.
716 Each treat of RNA sequencing is performed by using three biological repetitions.
717
718 **Hi-C library construction and sequencing**
719 The eggs of Mh were used to construct the Hi-C library according to previously described
720 method with appropriate modifications(44). Briefly, approximately 50 thousand newly collected
721 eggs were pelleted and cross-linked in a 1.5% final concentration (v/v) formaldehyde (Sigma)
722 for 30 min, followed de-crosslinking, eggs were homogenized and digested by using MboI
723 (New England Biolabs). DNA was extracted after the addition of biotin, end-filling and ligation.
724 Subsequently, the DNA was sheared and removed from the unligated fragment ends biotin
725 mark by using T4 DNA polymerase. After biotinylated fragment pull-down, the target DNA was
726 used to construct the Hi-C library by using End Prep Mix 4 from VAHTSTM Universal DNA
727 Library Prep Kit for Illumina® ND607 (Vazyme, Nanjing, China), and then sequenced on
728 Illunima NovaSeq platform with 150 bp paired-end reads.
729
730 **Chromosome-level genome assembly**
731 To obtain a high quality Mh genome, through the Pacbio data, we performed de novo genome
732 assembly by using Canu (v1.9)(67) with default parameters. The initial assembled contigs
733 were polished with Illumina short reads for 5 rounds by using BWA (v0.7.17)(68), SAMtools,
734 sambamba (v0.7.1)(69), and pilon (v1.23)(70). Then, the Hi-C reads were aligned into the
735 corrected contigs by using Juicer (v1.5.7) pipeline(71). The 3D-DNA (v180419) pipeline(72)
736 was used to construct the chromosome-level scaffolds with parameter of -r 0, and we finally
737 obtained the MhF1-2 genome with 99.18% sequences clustered into 16 chromosomes.
738
739 **Genome annotation**
740 The egg, J2, J3J4, and female stages of Mh were collected to performed RNA-seq and
741 subsequently use to genome annotation. RepeatModeler(73) and RepeatMasker(74)
742 (http://www.repeatmasker.org) were used to soft-mask repetitive region of the assembled
743 genome. The RNA-seq data was aligned to the masked genome by using HISAT2 (v2.2.1)(75),
744 then, the BAM files were utilized to annotation based on ab initio prediction evidence by using
745 AUGUSTUS (v3.3.3)(76), GeneMark-ES (v4.64)(77), and BRAKER2 (v2.1.6)(78). On the
746 other hand, the RNA-seq data were de novo assembled using Trinity (v2.8.5)(79), and the
747 assembled transcripts were used to the following integrated by PASA (v2.4.1)(80). The file

748 augustus.hints.gff3 from Braker2 and the file pasa_assemblies.gff3 from PASA were used to
749 integrate all evidence to obtain a final gene structure information by using EVidenceModeler
750 (v1.1.1)(80). For the functional annotation, HMMER(81) was used to scan all the predicted
751 proteins conserve domains based on Pfam database, and eggNOG-mapper (v2.0.1)(82) was
752 used to perform the KEGG and GO annotation. For secreted protein prediction, we considered
753 the proteins with signal peptide but without transmembrane domain were secreted proteins.
754 The signal peptides were predicted by SignalP (v5.0)(83), and the transmembrane domains
755 were identified by using TMHMM (2.0c)(84). The transposable elements (TEs) were predicted
756 by using EDTA (v2.0.0) pipeline(85).
757
758 **6mA identification and analysis by SMRT sequencing**
759 We use SMRTLink-7.0.1 (http://www.pacb.com/support/software-downloads/) to identify the
760 6mA modification in WHF4-1, Mg, and Mh genome. The SMRT sequencing reads were
761 aligned to the genome by pbmm2, and the 6mA modification sites were identified by
762 ipdSummary with the following options: --methylFraction, --minCoverage 3, --identify m6A,
763 --bigwig, --csv. The 6mA sites with less than 50 or 15 coverage were filtered according to the
764 sequencing depth of each RKNs as described before(13, 17). For motifs identification, the
765 6mA sites were separated into three groups based on their methylation level (0-30%,
766 30%-70%, 70%-100%). We extracted 4 bp from the upstream and downstream sequences of
767 each 6mA site and used BEDtools (v2.29.2)(86) to acquire the fasta file and followed by using
768 MEME-ChIP to identify motifs for each group. 6mA peaks were loading to R package
769 ChIPseeker (v1.24.0)(87) for associated genes annotation. The genome-wide distribution of
770 6mA sites with different methylation levels was visualized using Circos (v0.69)(88). To
771 calculate the reads contamination rate of SMRT sequencing, we aligned the PacBio reads to
772 bacteria, fungi, and plant NCBI nt library, the aligned length more than 90% of the query reads
773 were considered as a valid alignment.
774
775 **6mA distribution density analysis**
776 The 6mA sites with different methylation levels were extracted into 6mAfilterHigh.bed,
777 6mAfilterMiddle.bed, and 6mAfilterLow.bed. We extended 4bp upstream and downstream of
778 the 6mA site to obtain the *_8bp.bed files for subsequent analysis. BEDtools bedtobam was
779 utilized to convert the *_8bp.bed files to *_8bp.bam files, and deeptools bamCoverage was
780 used to generate *_8bp.bw files from *_8bp.bam files. Finally, the BED files containing exon
781 and TE information, along with the *_8bp.bw files, were used to calculate the distribution
782 density of 6mA in the gene or TE region using computeMatrix, and plotProfile was employed to
783 visualize the results.
784
785 **DNA Dot blot**
786 The Hybond+ membranes were fully soaked in double distilled water, then soaked in 20 SSC
787 for 1h, sandwiched between two layers of filter paper and dried at 37 °C for 30 min. The
788 purified genomic DNA was heated at 95 °C for 5 min to denature DNA and immediately placed
789 on ice for 5 min and then 15 ng, 30 ng, and 50 ng DNA were loaded per dot on Hybond+
790 membranes. Membranes were air dry and placed them in the oven at 80 °C for 1 h, and
791 transferred into boxes with damp paper towels. DNA was then auto-crosslinked twice for 6

792 min in an Ultraviolet crosslinker (CL-100). The membrane was blocked for 2 h in 5% skim milk
793 TTBS. Membranes were incubated overnight at 4 °C with 6mA primary antibody (ab151-230,
794 Abcam) in 5% skim milk TTBS. After three times wash for 5 min with TTBS, the blots were
795 probed with secondary antibody in 5% skim milk TTBS for 1 h at room temperature. Blots were
796 washed three times for 5 min with TTBS and then performed chemiluminescence detection.
797 After the chemiluminescence is over, the membrane is directly used for methylene blue
798 staining. (I) Immerse the membrane in 10mL of 1× methylene blue solution, stain for 3min on a
799 shaker at room temperature, and wash the membrane twice with double distilled water for 5
800 minutes each time; stain again with methylene blue solution for 3min and wash the membrane
801 twice with double distilled water for 5 minutes each time. Soak in TBST overnight at 4℃; (II)
802 Stain with methylene blue solution for 5min, wash three times with double distilled water for 5
803 minutes each time. Take photos in the gel imaging instrument/camera.
804
805 **LC–MS/MS analysis of 6mA**
806 The LC-MS/MS was performed as described before(13). Briefly, the nematodes genomic DNA
807 was denatured at 100 °C for 3 min, and chilled in ice for 2 min immediately. Aspirate 26 μl of
808 denatured DNA, add 1 μl of S1 nuclease, 3.2 μl of buffer, and treated at 37 °C overnight.
809 One-tenth volume of 1M NH_4HCO_3 and 1 μl venom phosphodiesterase I (Sigma) was added to
810 the solution and incubation at 37 °C for 2h. Finally, 1 U of alkaline phosphatase from *E. coli*
811 (Sigma) was added to the solution at 37 °C for 2h. The digested genomic DNA was diluted
812 two-fold with nuclease-free H_2O and filtered through 0.22 μm filter. To determine the peak
813 position of each nucleoside, the nucleoside standards including N6-methyldeoxyadenosine
814 and deoxyadenosine nucleoside were used to perform the reverse-phase ultra-performance
815 liquid chromatography on a C18 column (Agilent), with online mass spectrometry detection
816 using triple-quadrupole tandem mass spectrometer (Shimadzu, LC-MS 8050) set to multiple
817 reaction monitoring (MRM) in positive electrospray ionization mode. Simultaneous detection of
818 standards and samples using established methods base ion mass transitions of 266.1-150.0
819 for 6mA and 252.1-136.0 for A, and calculate the ratio of 6mA/A.
820
821 **RNA interference *in vitro***
822 We select about 300 bp conserved regions as RNAi target fragments. The PCR primers used
823 to amplify the RNAi target fragment template are as follows: minmad-1 F:
824 5'-GGTGGAATAATAAGTGGCTT-3', minmad-1 R: 5'-CTGATTGTGGAATTATTTTC-3';
825 minmad-2 F: 5'-CCTCAATTTATTTCGGAAGC-3', minmad-2 R:
826 5'-CCTGTCCAGGCAAATATTCA-3'; Mi_23849.1 F: 5'-GGATAGAAAAATGTCTGTTG-3',
827 Mi_23849.1 R: 5'-GCAGCATCAGGAAGGAAATC-3'; gfp F:
828 5'-GAGTGCCATGCCCGAAGGTTA-3', gfp R: 5'-GGTCTGCTAGTTGAACGCTTCC-3'.
829 Mg_06820 F: 5'-GAAACAGAAGAAGCAAAT-3', Mg_06820 R:
830 5'-AGTAGAAATCATTGGAAAG-3'; Mg_00565 F: 5'-GTATTGGATTAAATAATTTCTTC-3',
831 Mg_00565 R: 5'-TTTGTATAGATTCTTCACTAA-3'. We synthesized dsRNA using the T7
832 RNAi Transcription Kit-Box 1 (Vazyme, China, Cat. TR102-02). We followed the protocol for
833 dsRNA synthesis and diluted the concentration of dsRNA to 2 μg/μl. The potential 6mA
834 demethylase in vitro interference experiment was performed using WHF4-1 eggs. About
835 10,000 WHF4-1 eggs were sterilized and suspended in 100 μl of nuclease-free water, and an

836 equal volume of dsRNA solution was added to make the final concentration of dsRNA to 1
837 μg/μl. After 60 hours of incubation at room temperature with 15 rpm rotation, the disturbed
838 eggs were divided into two parts, one was used for qRT-PCR to detect the interference
839 efficiency of the target gene, and the other was used to extract DNA to detect 6mA content by
840 mass spectrometry. Three biological replicates were performed for each experiment, dsGFP
841 was used as control.
842
843 **RNA-seq analysis**
844 The RNA-seq data of *C. elegans* were downloaded from SRA database (accession number
845 SRR6125151-SRR6125153). The raw reads of RNA-seq were cleaned by Cutadapt, the PCR
846 duplications were removed by using Picard. We use STAR [84] to align the reads to RKNs
847 genome and use RSEM(89) to calculate the TPM and FPKM value of each gene. For
848 differentially expressed genes (DEGs) analysis, HISAT2 was used to align the RNA-seq data
849 to the RKNs genome, then use SAMtools to convert the SAM files to BAM files and sort them,
850 and finally use HTSeq-count (v0.13.5)(90) to calculate the expression count number of each
851 gene. The count number was input into DESeq2 (v1.28.1)(91) to standardize and acquire the
852 DEGs. Differentially expressed genes (DEGs) were identified using DESeq2, applying an
853 adjusted p-value (FDR) < 0.05 and an absolute log2foldchange > 1 as thresholds.
854 Comparisons of gene expression (TPM) between groups were performed using the Wilcoxon
855 rank sum test, as TPM values showed non-normal distributions and unequal variances. Each
856 treatment was analyzed with three biological replicates. The expression module analysis of
857 secreted proteins was performed by using Mfuzz (v2.48.0)(92) and visualization by using R
858 package pheatmap (v1.0.12). The GO and Pfam enrichment analysis were performed by
859 python script and visualization by using R package ggplot2 (v3.3.3).
860
861 **Demethylase assays**
862 *In vitro* demethylase activity experiments were performed using purified potential demethylase
863 proteins of MiNMAD-1/2. The demethylase assays were performed as previously
864 described(13). In brief, a triplicate of a 50 μl volumes containing 1 μg WHF4-1 gDNA and 1 mg
865 recombinant protein in a reaction mixture (50 mM HEPES (pH 7.0), 50 mM KCl, 2 mM $MgCl_2$, 2
866 mM ascorbic acid, 1 mM α-KG, and 200 mM $(NH)_4Fe(SO)_4$) were used to perform the reaction.
867 After 1h hold at 37 °C, the reactions were stopped by adding 5mM EDTA and denatured at
868 100 °C for 3 min followed by chilling on ice for 2 min. The products of reactions were used to
869 Dot blot and LC-MS/MS to determine the 6mA contents after putative demethylase treated.
870
871 **Verification of nematode endogenous 6mA demethylase**
872 About 50 μl WHF4-1 eggs were collected and suspended in 200 μl nematode lysis buffer (50
873 mM HEPES, 150 mM NaCl, 10% glycerol, 1% Triton X-100, 1.5 mM $MgCl_2$, and 1 mM EGTA)
874 with proteinase inhibitor. After adding 100 mg of 1 mm diameter zirconia microspheres to the
875 suspension, the samples were crushed by a tissue grinder (JXFSTPRP-24L, Shanghaijingxin
876 Experimental technology, China), and the oscillation frequency was 70 Hz for 30 seconds, and
877 the repetition was repeated 5 times. Suck up 20 μl suspension into a new 1.5 ml centrifuge
878 tube, and add 64 μl ddH_2O, 10 μl reaction mixture, 1 μl protease inhibitor (Roche), 5 μl 20 μM
879 oligo DNA. The suspension was incubated with rotation at 12 rpm for 3-6 hours at 28 °C. To

separate the oligo DNA from Mi's own DNA, the biotin-labeled oligo DNA was pulled down using Dynabeads MyOne Streptavidin C1 beads (Thermo Fisher Scientific). 100 μl 2× BB (10 mM Tris-HCl (pH 7.5); 1 mM EDTA; 2 M NaCl) suspended Dynabeads MyOne Streptavidin C1 beads were mixed with the suspension and incubated at room temperature for 30 min with rotation (15 rpm). The beads with biotin marked DNA were washed three times with 300 μl TWB (5 mM Tris-HCl (pH 7.5); 0.5 mM EDTA; 1 M NaCl; 0.05% Tween 20) and incubated at 55 °C for 2 min. Added 27 μl ddH_2O to resuspend the beads, treat them in a dry bath at 98 °C for 10 minutes, centrifuge and collect the supernatant after magnetic stand separation. The experiment of treating oligo DNA with purified potential demethylase is the same as the above method, and the eggs suspension should be replaced with purified protein.

We noticed that the 6mA content of the control group was as high as about 40%, which was quite different from the 6mA content of the designed oligo DNA. We suspect that the increased ratio of 6mA is due to the degradation of part oligo DNA by nucleases present in the environment. Nevertheless, the experimental group and the control group still showed a significant difference in 6mA content. The method of 6mA content detection is consistent with that described above, and the oligo DNA sequence modified with 6mA, and biotin are shown as below:

Oligo name	Oligo sequence
6mA_motif	GGGAATTTCCCGGCGATTTGA(N6-Me-dA)GGTAATCGCCGGGAAATT(biotin)CCC

Mi-CRT polyclonal antibody preparation and western blot assays

All the work of polyclonal antibody preparation was performed by Friendbio Science & Technology (Wuhan, China). Briefly, the purified Mi-CRT protein was used to immunize rabbits intradermally for antiserum production, and gel specific purification was used to purify the antibody. For western blot, the WHF4-1 eggs and females were collected and homogenate as above. The protein concentration of the suspended was determined by using the BCA Kit (Beyotime, China). Proteins were separated on a 10% SDS-PAGE followed by blotting on PVDF membranes (Biosharp, China). The membranes were blocked 2h in 5% skim milk TTBS and probed with the Mi-CRT antibody or β-actin (Proteintech, China, Cat No.: 66009-1-Ig) overnight. The secondary antibody and detection were performed as described in Dot blot.

Demethylase prediction

We aligned the proteins sequence of WHF4-1 to the protein NMAD-1 of *C. elegans* by using a loose e-values by using blastp (v2.10.1)(93). The first three proteins on the alignment were selected as candidate demethylases. On the other hand, we performed Pfam domain annotation on all the proteins of WHF4-1 and found that 6 of them have the 2OG-FeII_Oxy_2 domain with potential 6mA demethylase function. Every three of these 9 candidate genes are alleles of each other, the coverage between alleles is 100%, and the minimum identity is 96%, therefore, we selected one of the three alleles for further validation studies.

Transgenic plant construct

920 Nicotiana benthamiana was used to generate transgenic tobacco following the method of
921 Agrobacterium-mediated genetic transformation of leaf discs(94). We selected the same
922 segment as the above *in vitro* RNA interference as the segment for constructing transgenic
923 plants expressing dsRNA. The Agrobacterium EHA105 was inoculated into YEB medium and
924 cultured at 28 °C until OD600 up to 0.6-0.8. Put the tobacco leaf discs for about 6-7 weeks into
925 the Agrobacterium suspension and soak for 10min and culture in the dark at 28 °C for 2-4 days.
926 The explants were transferred to the Murashige and Skoog (MS) medium (with 1.0 mg/L
927 hormones Benzylaminopurine, 0.1 mg/L Indole acetic acid, 100 mg/L antibiotics kanamycin,
928 and 500 mg/L cefotaxime), and cultured under a light intensity of 25 μmol m^{-2} s^{-1} at 25 °C. After
929 4-5 weeks of selective culture, the explants will regenerate shoot buds and then transferred to
930 fresh selective medium. When the shoot buds grow to 3-4 cm, transfer to the rooting medium
931 (1/2 MS medium with the same concentration of antibiotics), and the roots will grow about 2-3
932 weeks. Using qRT-PCR to confirm putative T0 transgenic plants with specific primers as below.
933 Further, PCR-positive plant was cultured in glass house to obtain a homozygous T1
934 generation. Tomato transformation was performed using the 'Moneymaker' cultivar, following
935 the same method as used for tobacco transformation. Cotyledons and hypocotyls from
936 5-day-old tomato seedlings were used for the transformation. The rice transgenic was
937 completed by Wuhan Towin Biotechnology Co., Ltd.

Primer name	Primer sequence
MiNMAD-1 F	TACCTCAATAATGCGGCTTGTT
MiNMAD-1 R	ACTCTCTTCATTAGCCAGGATTTC
MiNMAD-2 F	CCTCAATTTATTTCGGAAGCAGAA
MiNMAD-2 R	TCTAACCACATCGGCAATTCTT
Mi_23849.1 F	TCCGAGACAATCTTTACCTGATGA
Mi_23849.1 R	AAATCGCCCAAGCCTAGACTA

938 **Acknowledgements**
939 We thank Huazhong Agricultural University for technical support; Weiguo Lu of Henan
940 Academy of Agricultural Sciences for providing cyst nematode X12 material; Min Hu of
941 Huazhong Agricultural University for providing the *Haemonchus contortus* species; Xiaoli Guo
942 of Huazhong Agricultural University for providing the cyst nematodes Hg3 and Hg5 species;
943 Fengjuan Zhang of Hubei University for providing the *Aphelenchus avenae* and
944 *Bursaphelenchus xylophilus* species.
945
946 **References**
947 1. A. Zemach, I. E. McDaniel, P. Silva, D. Zilberman, Genome-wide evolutionary analysis
948 of eukaryotic DNA methylation. *Science* **328**, 916-919 (2010).
949 2. D. Wion, J. Casadesus, N6-methyl-adenine: an epigenetic signal for DNA-protein
950 interactions. *Nat Rev Microbiol* **4**, 183-192 (2006).
951 3. M. N. Giacomodonato, S. H. Sarnacki, M. N. Llana, M. C. Cerquetti, Dam and its role
952 in pathogenicity of *Salmonella enterica*. *The Journal of Infection in Developing*
953 *Countries* **3**, 484-490 (2009).
954 4. J. López-Garrido, J. Casadesús, Regulation of Salmonella enterica pathogenicity
955 island 1 by DNA adenine methylation. *Genetics* **184**, 637-649 (2010).

956 5. M. N. Giacomodonato *et al.*, Dam methylation regulates the expression of
957 SPI-5-encoded sopB gene in *Salmonella enterica* serovar Typhimurium. *Microbes and*
958 *Infection* **16**, 615-622 (2014).
959 6. M. N. Giacomodonato *et al.*, Impaired synthesis and secretion of SopA in *Salmonella*
960 Typhimurium dam mutants. *FEMS microbiology letters* **292**, 71-77 (2009).
961 7. J. A. Banas, S. Biswas, M. Zhu, Effects of DNA methylation on expression of virulence
962 genes in *Streptococcus mutans*. *Applied and environmental microbiology* **77**,
963 7236-7242 (2011).
964 8. Y. N. Srikhanta *et al.*, Phasevarion-regulated virulence in the emerging pediatric
965 pathogen *Kingella kingae*. *Infection and Immunity* **85**, 10.1128/iai. 00319-00317
966 (2017).
967 9. S. Falker, M. A. Schmidt, G. Heusipp, DNA methylation in *Yersinia enterocolitica*: role
968 of the DNA adenine methyltransferase in mismatch repair and regulation of virulence
969 factors. *Microbiology* **151**, 2291-2299 (2005).
970 10. S. Han *et al.*, DNA Methyltransferase regulates nitric oxide homeostasis and virulence
971 in a chronically adapted *Pseudomonas aeruginosa* strain. *MSystems* **7**,
972 e00434-00422 (2022).
973 11. T. M. Nye *et al.*, DNA methylation from a Type I restriction modification system
974 influences gene expression and virulence in *Streptococcus pyogenes*. *PLoS*
975 *pathogens* **15**, e1007841 (2019).
976 12. Z. Miao *et al.*, BcMettl4-mediated DNA adenine N 6-methylation (6mA) is critical for
977 virulence of *Botrytis cinerea*. *Frontiers in Microbiology*, 2155 (2022).
978 13. E. L. Greer *et al.*, DNA Methylation on N6-Adenine in *C. elegans*. *Cell* **161**, 868-878
979 (2015).
980 14. Z. Liu, Y. Li, X. Zhang, DNA methylation on C5-Cytosine and N6-Adenine in the
981 *Bursaphelenchus xylophilus* genome. *BMC genomics* **24**, 671 (2023).
982 15. G. Zhang *et al.*, N6-methyladenine DNA modification in *Drosophila*. *Cell* **161**, 893-906
983 (2015).
984 16. Y. Fu *et al.*, N6-methyldeoxyadenosine marks active transcription start sites in
985 *Chlamydomonas*. *Cell* **161**, 879-892 (2015).
986 17. S. J. Mondo *et al.*, Widespread adenine N6-methylation of active genes in fungi. *Nat*
987 *Genet* **49**, 964-968 (2017).
988 18. C. Lax *et al.*, Symmetric and asymmetric DNA N6-adenine methylation regulates
989 different biological responses in *Mucorales*. *Nature Communications* **15**, 6066 (2024).
990 19. C. Zhou *et al.*, Identification and analysis of adenine N(6)-methylation sites in the rice
991 genome. *Nat Plants* **4**, 554-563 (2018).
992 20. Q. Zhang *et al.*, N(6)-Methyladenine DNA methylation in Japonica and Indica rice
993 genomes and its association with gene expression, plant development, and stress
994 responses. *Mol Plant* **11**, 1492-1508 (2018).
995 21. Z. Liang *et al.*, DNA N(6)-Adenine methylation in *Arabidopsis thaliana*. *Dev Cell* **45**,
996 406-416 e403 (2018).
997 22. C. L. Xiao *et al.*, N(6)-Methyladenine DNA modification in the human genome. *Mol*
998 *Cell* **71**, 306-318 e307 (2018).
999 23. Y. Sheng *et al.*, Semiconservative transmission of DNA N6-adenine methylation in a

1000 unicellular eukaryote. *Genome Research* (2024).
1001 24. X. Liu *et al.*, N6-methyladenine is incorporated into mammalian genome by DNA
1002 polymerase. *Cell research* **31**, 94-97 (2021).
1003 25. C. Lyu *et al.*, Rare and misincorporated DNA N6-methyladenine is a hallmark of
1004 cytotoxic stresses for selectively stimulating the stemness and proliferation of
1005 glioblastoma cells. *Cell Discovery* **8**, 39 (2022).
1006 26. Q. Xie *et al.*, N(6)-methyladenine DNA modification in glioblastoma. *Cell* **175**,
1007 1228-1243 e1220 (2018).
1008 27. C. Shen, K. Wang, X. Deng, J. Chen, DNA N(6)-methyldeoxyadenosine in mammals
1009 and human disease. *Trends Genet* **38**, 454-467 (2022).
1010 28. L. Luo *et al.*, DNA 6mA demethylase ALKBH1 orchestrates fatty acid metabolism and
1011 suppresses diet-induced hepatic steatosis. *Cell Mol Gastroenterol Hepatol* **14**,
1012 1213-1233 (2022).
1013 29. C. Ma *et al.*, N6-methyldeoxyadenine is a transgenerational epigenetic signal for
1014 mitochondrial stress adaptation. *Nature Cell Biology* **21**, 319-327 (2019).
1015 30. S. Y. Wang *et al.*, The demethylase NMAD-1 regulates DNA replication and repair in
1016 the *Caenorhabditis elegans* germline. *PLoS Genet* **15**, e1008252 (2019).
1017 31. K. Zhu, J. Reiser, ALKBH1 reduces DNA N6-methyladenine to allow for vascular
1018 calcification in chronic kidney disease. *J Clin Invest* **131** (2021).
1019 32. B. Yao *et al.*, Active N(6)-methyladenine demethylation by DMAD regulates gene
1020 expression by coordinating with polycomb protein in neurons. *Mol Cell* **71**, 848-857
1021 e846 (2018).
1022 33. M. Osorio-Concepcion, C. Lax, E. Navarro, F. E. Nicolas, V. Garre, DNA methylation
1023 on N6-adenine regulates the hyphal development during dimorphism in the
1024 early-diverging fungus *Mucor lusitanicus*. *J Fungi (Basel)* **7** (2021).
1025 34. Y. Kong *et al.*, Critical assessment of DNA adenine methylation in eukaryotes using
1026 quantitative deconvolution. *Science* **375**, 515-522 (2022).
1027 35. P. Abad *et al.*, Genome sequence of the metazoan plant-parasitic nematode
1028 *Meloidogyne incognita*. *Nat Biotechnol* **26**, 909-915 (2008).
1029 36. J. T. Jones *et al.*, Top 10 plant-parasitic nematodes in molecular plant pathology. *Mol*
1030 *Plant Pathol* **14**, 946-961 (2013).
1031 37. P. Castagnone-Sereno, E. G. Danchin, L. Perfus-Barbeoch, P. Abad, Diversity and
1032 evolution of root-knot nematodes, genus *Meloidogyne*: new insights from the genomic
1033 era. *Annu Rev Phytopathol* **51**, 203-220 (2013).
1034 38. T. Hewezi, T. J. Baum, Manipulation of plant cells by cyst and root-knot nematode
1035 effectors. *Mol Plant Microbe Interact* **26**, 9-16 (2013).
1036 39. L. Perfus-Barbeoch *et al.*, Elucidating the molecular bases of epigenetic inheritance in
1037 non-model invertebrates: the case of the root-knot nematode *Meloidogyne incognita*.
1038 *Front Physiol* **5**, 211 (2014).
1039 40. R. Hassanaly-Goulamhoussen *et al.*, Chromatin landscape dynamics in the early
1040 development of the plant parasitic nematode *Meloidogyne incognita*. *Front Cell Dev*
1041 *Biol* **9**, 765690 (2021).
1042 41. M. R. Atighi, B. Verstraeten, T. De Meyer, T. Kyndt, Genome-wide shifts in histone
1043 modifications at early stage of rice infection with *Meloidogyne graminicola*. *Molecular*

1044 *Plant Pathology* **22**, 440-455 (2021).
1045 42. T. Hewezi, Epigenetic mechanisms in nematode-plant interactions. *Annu Rev*
1046 *Phytopathol* **58**, 119-138 (2020).
1047 43. L. Pratx *et al.*, Genome-wide expert annotation of the epigenetic machinery of the
1048 plant-parasitic nematodes *Meloidogyne* spp., with a focus on the asexually
1049 reproducing species. *BMC Genomics* **19**, 321 (2018).
1050 44. D. Dai *et al.*, Unzipped chromosome-level genomes reveal allopolyploid nematode
1051 origin pattern as unreduced gamete hybridization. *Nature Communications* **14**, 7156
1052 (2023).
1053 45. C. H. Opperman *et al.*, Sequence and genetic map of *Meloidogyne hapla*: A compact
1054 nematode genome for plant parasitism. *Proceedings of the National Academy of*
1055 *Sciences* **105**, 14802-14807 (2008).
1056 46. P. A. Jones, Functions of DNA methylation: islands, start sites, gene bodies and
1057 beyond. *Nature reviews genetics* **13**, 484-492 (2012).
1058 47. Z. Hao *et al.*, N(6)-deoxyadenosine methylation in mammalian mitochondrial DNA.
1059 *Mol Cell* **78**, 382-395 e388 (2020).
1060 48. H. M. Robertson, J. H. Thomas, The putative chemoreceptor families of *C. elegans*.
1061 *WormBook* 10.1895/wormbook.1.66.1, 1-12 (2006).
1062 49. C. Jiang *et al.*, An expanded subfamily of G-protein-coupled receptor genes in
1063 *Fusarium graminearum* required for wheat infection. *Nat Microbiol* **4**, 1582-1591
1064 (2019).
1065 50. J. Shang, Y. Shang, G. Tang, C. Wang, Identification of a key G-protein coupled
1066 receptor in mediating appressorium formation and fungal virulence against insects. *Sci*
1067 *China Life Sci* **64**, 466-477 (2021).
1068 51. C. Kumari *et al.*, Molecular characterization of FMRFamide-like peptides in
1069 *Meloidogyne graminicola* and analysis of their knockdown effect on nematode
1070 infectivity. *Gene* **619**, 50-60 (2017).
1071 52. J. Jumper *et al.*, Highly accurate protein structure prediction with AlphaFold. *Nature*
1072 **596**, 583-589 (2021).
1073 53. N. K. Whiteman, A. D. Gloss, Parasitology: Nematode debt to bacteria. *Nature* **468**,
1074 641-642 (2010).
1075 54. R. K. Slotkin, R. Martienssen, Transposable elements and the epigenetic regulation of
1076 the genome. *Nature reviews genetics* **8**, 272-285 (2007).
1077 55. J. D. Hollister, B. S. Gaut, Epigenetic silencing of transposable elements: a trade-off
1078 between reduced transposition and deleterious effects on neighboring gene
1079 expression. *Genome research* **19**, 1419-1428 (2009).
1080 56. S. P. Klein, S. N. Anderson, The evolution and function of transposons in epigenetic
1081 regulation in response to the environment. *Curr Opin Plant Biol* **69**, 102277 (2022).
1082 57. Y. F. Wei, K. C. Carter, R. P. Wang, B. K. Shell, Molecular cloning and functional
1083 analysis of a human cDNA encoding an *Escherichia coli* AlkB homolog, a protein
1084 involved in DNA alkylation damage repair. *Nucleic Acids Res* **24**, 931-937 (1996).
1085 58. B. I. Fedeles, V. Singh, J. C. Delaney, D. Li, J. M. Essigmann, The AlkB family of Fe
1086 (II)/α-ketoglutarate-dependent dioxygenases: repairing nucleic acid alkylation damage
1087 and beyond. *Journal of Biological Chemistry* **290**, 20734-20742 (2015).

1088 59. T. P. Wu *et al.*, DNA methylation on N(6)-adenine in mammalian embryonic stem cells.
1089 *Nature* **532**, 329-333 (2016).
1090 60. M. Martin, Cutadapt removes adapter sequences from high-throughput sequencing
1091 reads. *EMBnet. journal* **17**, 10-12 (2011).
1092 61. B. Langmead, S. L. Salzberg, Fast gapped-read alignment with Bowtie 2. *Nat Methods*
1093 **9**, 357-359 (2012).
1094 62. H. Li *et al.*, The Sequence Alignment/Map format and SAMtools. *Bioinformatics* **25**,
1095 2078-2079 (2009).
1096 63. Y. Zhang *et al.*, Model-based analysis of ChIP-Seq (MACS). *Genome Biol* **9**, R137
1097 (2008).
1098 64. F. Ramirez, F. Dundar, S. Diehl, B. A. Gruning, T. Manke, deepTools: a flexible
1099 platform for exploring deep-sequencing data. *Nucleic Acids Res* **42**, W187-191 (2014).
1100 65. J. T. Robinson *et al.*, Integrative genomics viewer. *Nature biotechnology* **29**, 24-26
1101 (2011).
1102 66. P. Machanick, T. L. Bailey, MEME-ChIP: motif analysis of large DNA datasets.
1103 *Bioinformatics* **27**, 1696-1697 (2011).
1104 67. S. Koren *et al.*, Canu: scalable and accurate long-read assembly via adaptive k-mer
1105 weighting and repeat separation. *Genome Res* **27**, 722-736 (2017).
1106 68. H. Li, R. Durbin, Fast and accurate short read alignment with Burrows-Wheeler
1107 transform. *Bioinformatics* **25**, 1754-1760 (2009).
1108 69. A. Tarasov, A. J. Vilella, E. Cuppen, I. J. Nijman, P. Prins, Sambamba: fast processing
1109 of NGS alignment formats. *Bioinformatics* **31**, 2032-2034 (2015).
1110 70. B. J. Walker *et al.*, Pilon: an integrated tool for comprehensive microbial variant
1111 detection and genome assembly improvement. *PLoS One* **9**, e112963 (2014).
1112 71. N. C. Durand *et al.*, Juicer provides a one-click system for analyzing loop-resolution
1113 Hi-C experiments. *Cell Syst* **3**, 95-98 (2016).
1114 72. O. Dudchenko *et al.*, De novo assembly of the *Aedes aegypti* genome using Hi-C
1115 yields chromosome-length scaffolds. *Science* **356**, 92-95 (2017).
1116 73. J. M. Flynn *et al.*, RepeatModeler2 for automated genomic discovery of transposable
1117 element families. *Proc Natl Acad Sci U S A* **117**, 9451-9457 (2020).
1118 74. N. Chen, Using repeat masker to identify repetitive elements in genomic sequences.
1119 *Current protocols in bioinformatics* **5**, 4.10. 11-14.10. 14 (2004).
1120 75. D. Kim, J. M. Paggi, C. Park, C. Bennett, S. L. Salzberg, Graph-based genome
1121 alignment and genotyping with HISAT2 and HISAT-genotype. *Nat Biotechnol* **37**,
1122 907-915 (2019).
1123 76. M. Stanke *et al.*, AUGUSTUS: ab initio prediction of alternative transcripts. *Nucleic*
1124 *acids research* **34**, W435-W439 (2006).
1125 77. A. Lomsadze, V. Ter-Hovhannisyan, Y. O. Chernoff, M. Borodovsky, Gene
1126 identification in novel eukaryotic genomes by self-training algorithm. *Nucleic acids*
1127 *research* **33**, 6494-6506 (2005).
1128 78. T. Bruna, K. J. Hoff, A. Lomsadze, M. Stanke, M. Borodovsky, BRAKER2: automatic
1129 eukaryotic genome annotation with GeneMark-EP+ and AUGUSTUS supported by a
1130 protein database. *NAR Genom Bioinform* **3**, lqaa108 (2021).
1131 79. B. J. Haas *et al.*, De novo transcript sequence reconstruction from RNA-seq using the

1132 Trinity platform for reference generation and analysis. *Nature protocols* **8**, 1494-1512
1133 (2013).
1134 80. B. J. Haas *et al.*, Automated eukaryotic gene structure annotation using
1135 EVidenceModeler and the Program to Assemble Spliced Alignments. *Genome biology*
1136 **9**, 1-22 (2008).
1137 81. R. D. Finn, J. Clements, S. R. Eddy, HMMER web server: interactive sequence
1138 similarity searching. *Nucleic acids research* **39**, W29-W37 (2011).
1139 82. J. Huerta-Cepas *et al.*, Fast genome-wide functional annotation through orthology
1140 assignment by eggNOG-mapper. *Molecular biology and evolution* **34**, 2115-2122
1141 (2017).
1142 83. J. J. Almagro Armenteros *et al.*, SignalP 5.0 improves signal peptide predictions using
1143 deep neural networks. *Nature biotechnology* **37**, 420-423 (2019).
1144 84. S. Möller, M. D. Croning, R. Apweiler, Evaluation of methods for the prediction of
1145 membrane spanning regions. *Bioinformatics* **17**, 646-653 (2001).
1146 85. S. Ou *et al.*, Benchmarking transposable element annotation methods for creation of a
1147 streamlined, comprehensive pipeline. *Genome biology* **20**, 1-18 (2019).
1148 86. A. R. Quinlan, I. M. Hall, BEDTools: a flexible suite of utilities for comparing genomic
1149 features. *Bioinformatics* **26**, 841-842 (2010).
1150 87. G. Yu, L.-G. Wang, Q.-Y. He, ChIPseeker: an R/Bioconductor package for ChIP peak
1151 annotation, comparison and visualization. *Bioinformatics* **31**, 2382-2383 (2015).
1152 88. M. Krzywinski *et al.*, Circos: an information aesthetic for comparative genomics.
1153 *Genome Res* **19**, 1639-1645 (2009).
1154 89. B. Li, C. N. Dewey, RSEM: accurate transcript quantification from RNA-Seq data with
1155 or without a reference genome. *BMC bioinformatics* **12**, 1-16 (2011).
1156 90. S. Anders, P. T. Pyl, W. Huber, HTSeq—a Python framework to work with
1157 high-throughput sequencing data. *bioinformatics* **31**, 166-169 (2015).
1158 91. M. I. Love, W. Huber, S. Anders, Moderated estimation of fold change and dispersion
1159 for RNA-seq data with DESeq2. *Genome biology* **15**, 1-21 (2014).
1160 92. L. Kumar, M. E. Futschik, Mfuzz: a software package for soft clustering of microarray
1161 data. *Bioinformation* **2**, 5 (2007).
1162 93. S. F. Altschul *et al.*, Gapped BLAST and PSI-BLAST: a new generation of protein
1163 database search programs. *Nucleic acids research* **25**, 3389-3402 (1997).
1164 94. R. Horsch *et al.*, A simple and general method for transferring genes into plants.
1165 *science* **227**, 1229-1231 (1985).
1166

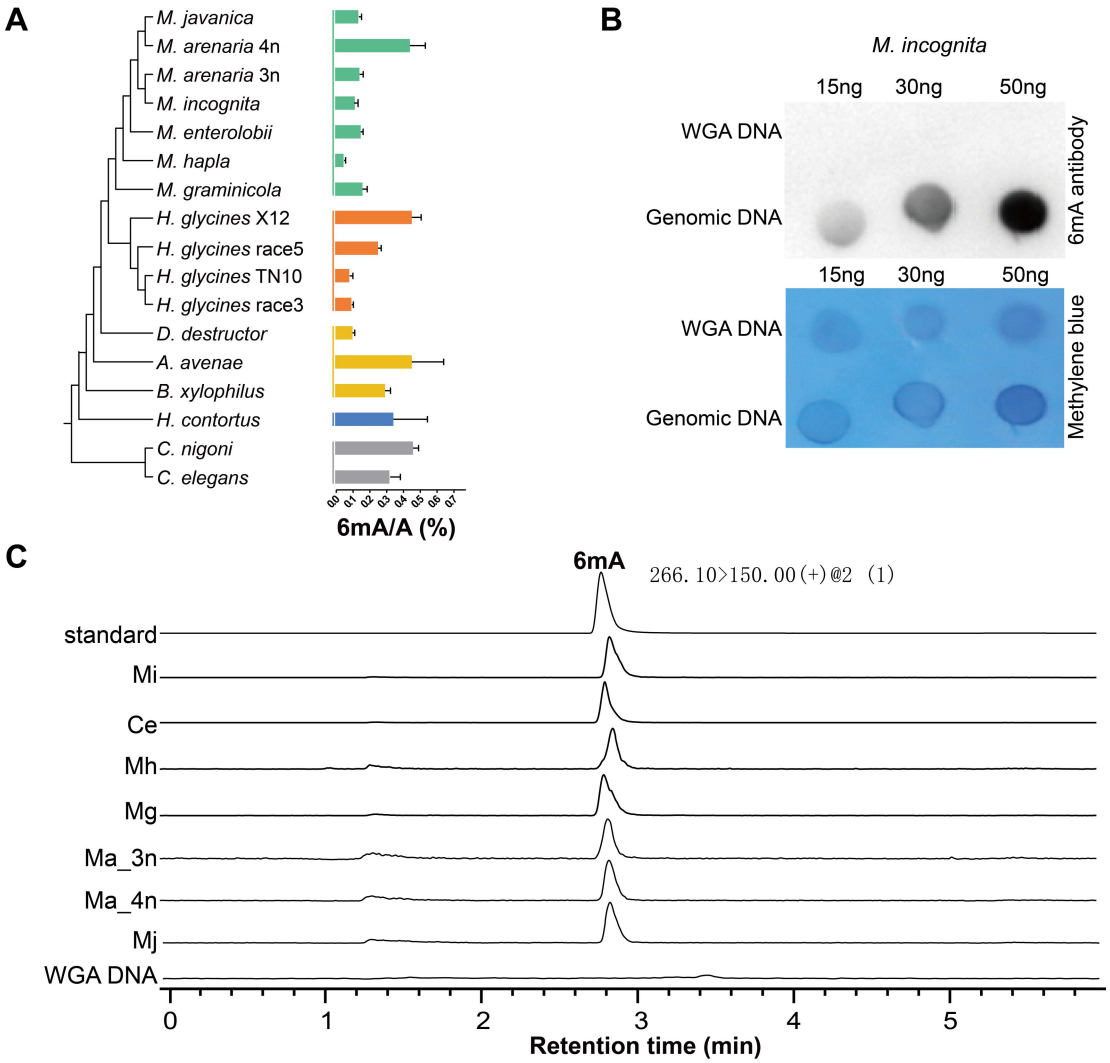

Figure 1. 6mA DNA methylation is widespread in nematode. (*A*), 6mA levels identified by LC-MS/MS in different nematodes. The green bar plot means 7 species of RKNs, the orange bar plot means 4 isolates of cyst nematodes, the yellow bar plot means migratory nematodes, the blue bar plot means animal-parasitic nematode, and the gray bar plot means free-living nematode. Three biological replicates per species. (*B*), The DNA 6mA Dot blot of *M. incognita,* the figure below shows the membrane after antibody hybridization and chemiluminescence, and then methylene blue staining. Whole genome amplified (WGA) DNA of the *M. incognita* genome, generated using Phi29 polymerase, was used as a negative control. (*C*), LC-MS/MS for 6mA standard and 6mA levels in genomic DNA purified from *M. incognita*, *C. elegans*, *M. hapla* (Mh), *M. graminicola* (Mg), *M. arenaria* 3n (Ma 3n), *M. arenaria* 4n (Ma 4n), and *M. javanica* (Mj), respectively. The WGA DNA was used as a negative control. All DNAs were extracted from nematode eggs.

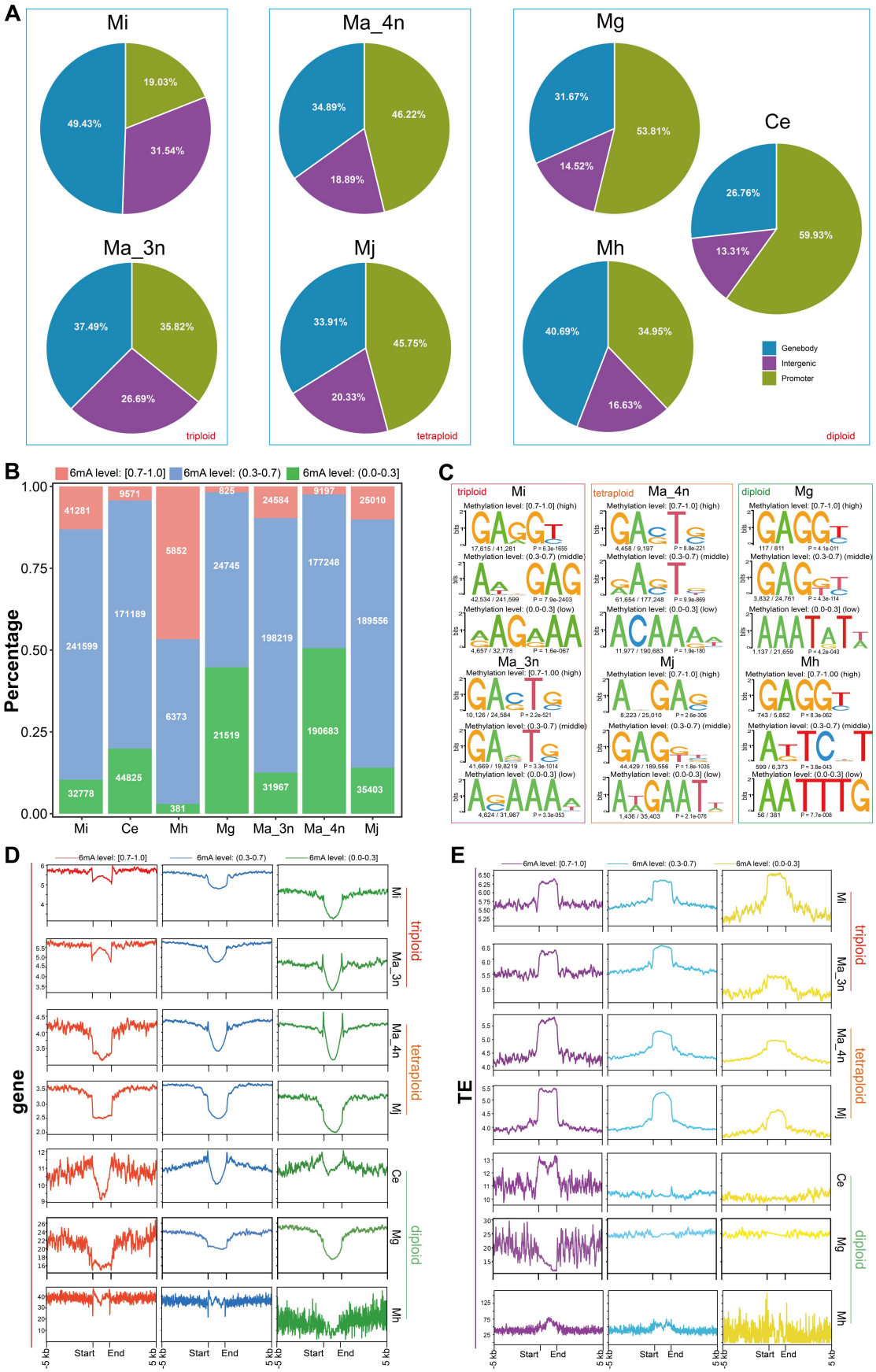

Figure 2. The distribution landscape of 6mA in RKNs genome. (*A*), The distribution ratio of 6mA in three nematodes promoter, gene body, and intergenic. *M. incognita* (Mi), *M. arenaria*

3n (Ma 3n), *M. arenaria* 4n (Ma 4n), *M. javanica* (Mj), *M. graminicola* (Mg), *M. hapla* (Mh), and *C. elegans*. The 1 kb region before the start codon is defined as the promoter. (*B*), Percentage of the different modification level categories of 6mA in Mi, Ma 3n, Ma 4n, Mj, Mg, and Mh, respectively. (*C*), The motif of different methylation categories of Mi, Ma 3n, Ma 4n, Mj, Mg, and Mh. (*D*) The distribution density of 6mA on gene regions within 100bp genome window (Mi, Ma 3n, Ma 4n, Mj, Ce, Mg, and Mh). (*E*) The distribution density of 6mA on transposable element (TE) region within 100bp genome window. *p* values were calculated by two-sided Wilcoxon rank sum tests. The y-axis represents the average number of 6mA per 100 bp genome window.

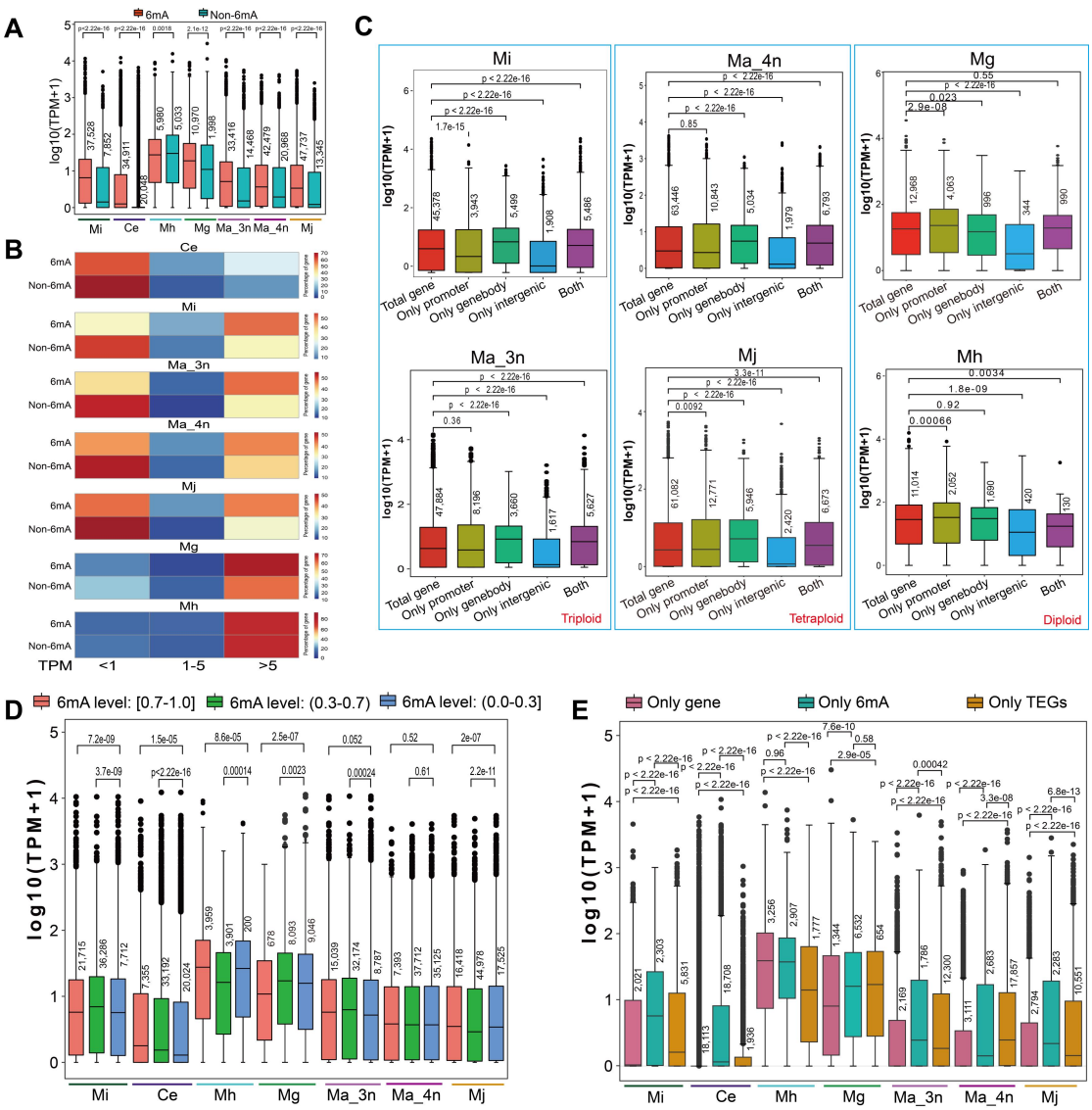

Figure 3. 6mA influences the genes expression level of nematodes. (*A*) The comparison of TPM value between 6mA-methylated (6mA) and unmethylated (Non-6mA) in Ce, Mi, Ma, Mj, Mg, and Mh. The gene with 6mA modification in the promoter, gene body, or intergenic region was defined as a 6mA-modified gene; otherwise, it was classified as an unmethylated gene. (*B*) The percentage of 6mA-methylated (6mA) and unmethylated (Non-6mA) genes at a given TPM level (<1, 1–5, and >5). (*C*) The comparison of expression levels between the genes modified by 6mA at different positions and total genes. (*D*) The comparison of genes expression level of different 6mA modification level categories in Mi, Ma 3n, Ma 4n, Mj, Ce, Mg, and Mh. (*E*) The gene expression comparing the gene only modified by 6mA (only 6mA), only TE nearby (only TE), and neither 6mA nor TE (only gene) in Mi, Mh, Mg, Ma 3n, Ma 4n, and Mj. In box plots, the central line represents the median, the box represents the 25% and 75% percentiles, and the whiskers represent 1.5 times the interquartile range beyond the box. N numbers were shown upon the box. *p* values were calculated by two-sided Wilcoxon rank sum tests.

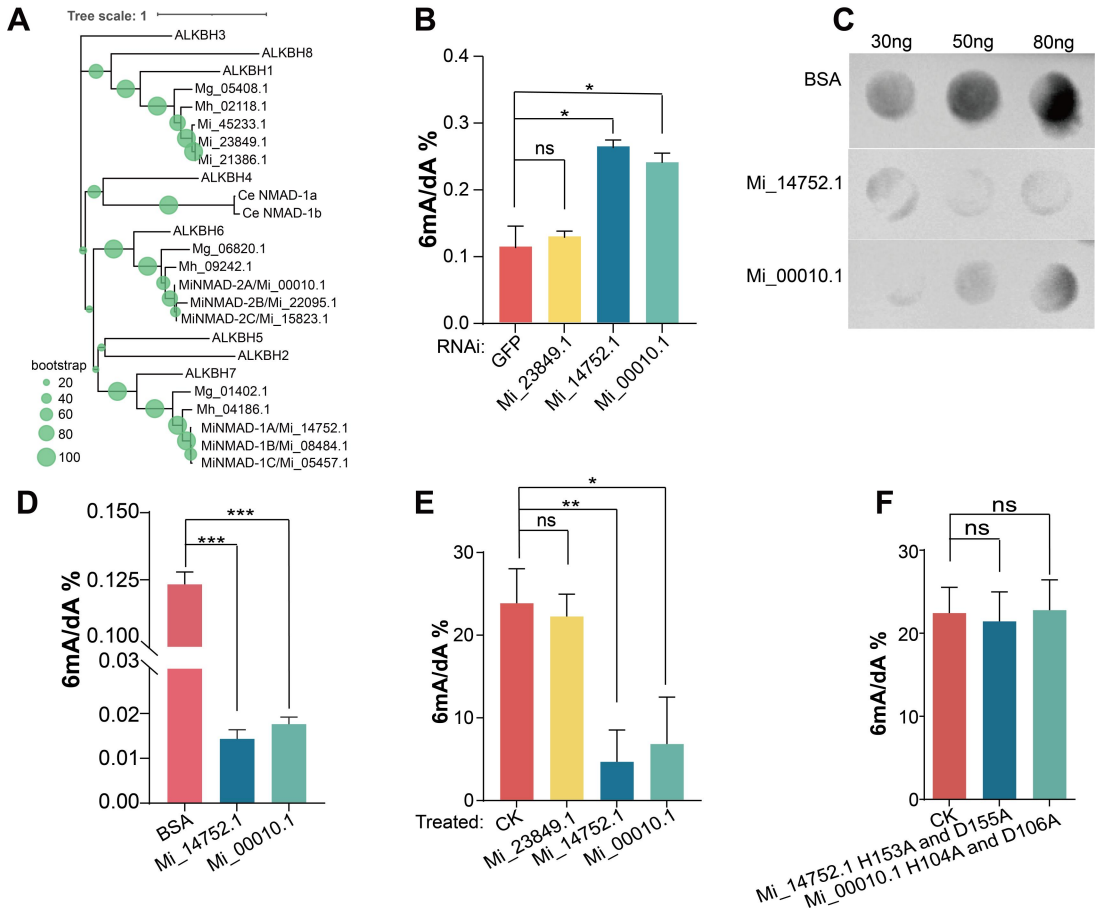

Figure 4. MiNMAD-1/2 are involved in 6mA demethylation in *M. incognita*. (*A*), The maximum-likelihood tree is constructed from the protein sequence of RKNs, *C. elegans* demethylase, and human ALKBH family members, bootstraps are shown in green dot. (*B*), Knockdown of 3 ALKBH family members present a significant increase of 6mA level in two of them (Mi_14752.1, Mi_00010.1). (*C*), In vitro demethylation assay showing that purified Mi_14752.1 and Mi_00010.1 proteins catalyze the removal of DNA methylation from Mi WHF4-1 egg genomic DNA, with BSA included as a negative control. (*D*), The 6mA contents of (*C*) were determined by LC-MS/MS. (*E*), LC-MSMS detected the oligo DNA with 6mA modified (G**A**G) was demethylated by purified MiNMAD-1/2 proteins *in vitro*. (*F*), Mutation of the catalytic domain of Mi_14752.1 and Mi_00010.1 abrogates the ability of them to demethylate 6mA premethylated oligos. *p* values were calculated by two-tailed unpaired Student's *t*-test. One star * means $p < 0.05$, two means $p < 0.01$, three means $p < 0.001$.

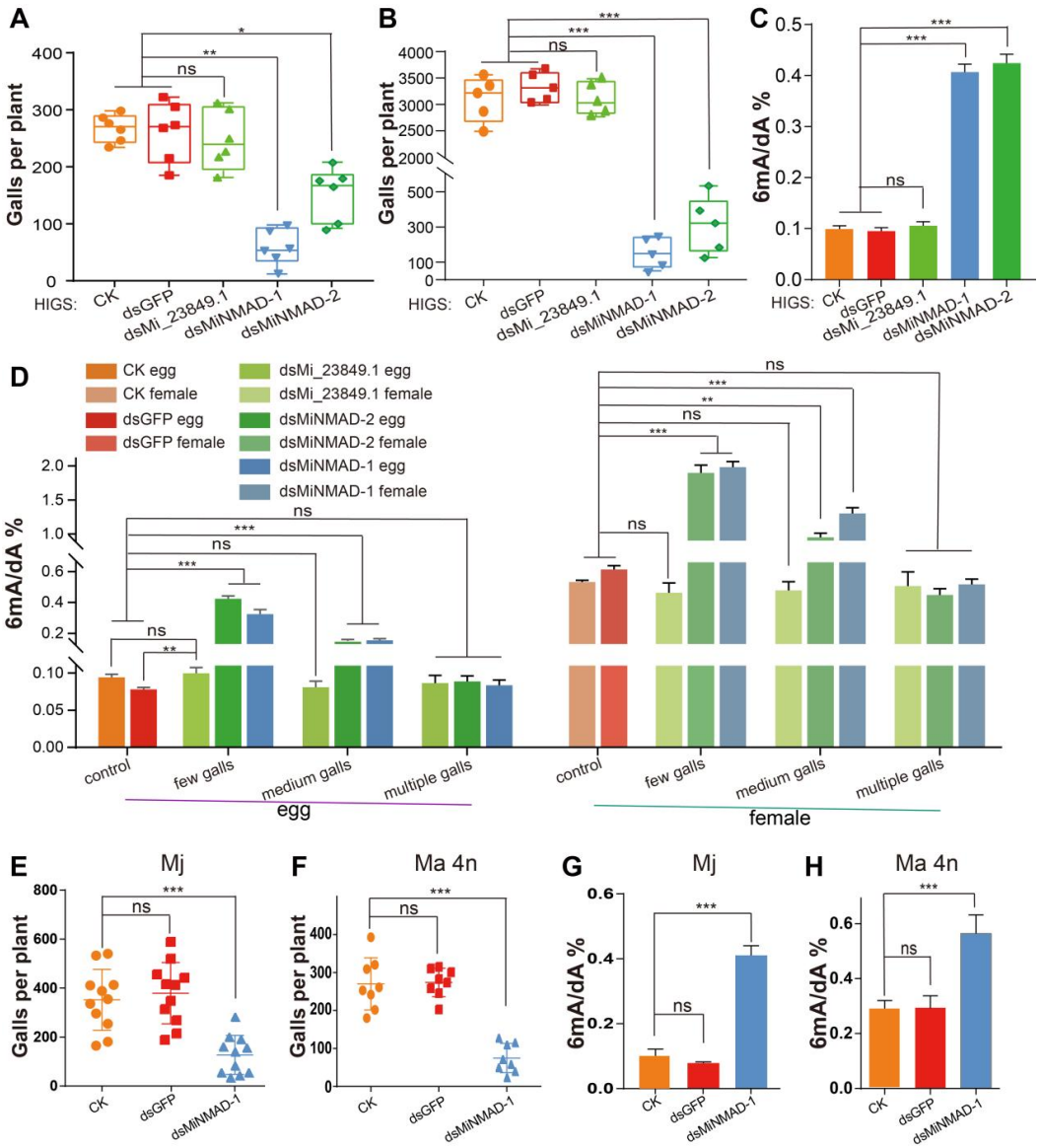

Figure 5. Host-induced gene silencing of *minmad-1* reduces the infectivity of polyploid RKNs. (*A*) Three weeks pot experiment of transgenic plants show a resistance of Mi for *minmad-1/2* RNAi, but no difference for *Mi_23849.1* RNAi. (*B*) Eight weeks pot experiment show an extremely significant resistance of expression *MiNMAD-1/2* dsRNA transgenic tobacco to Mi. (*C*) The 6mA level of Mi is significantly increased after infection of transgenic tobacco expression *minmad-1/2* dsRNA. (*D*) The number of galls was proportional to the methylation content in the corresponding Mi, and the level of 6mA in females was much higher than in eggs. (*E*) The number of galls after 1000 *M. javanica* (Mj) J2 infection two months of transgenic tobacco expressing *minmad-1* dsRNA. (*F*) The number of root-knots after 1000 M. arenaria 4n (Ma 4n) J2 infection of two months of transgenic tobacco expressing minmad-1 dsRNA. (*G*) The genomic DNA 6mA content of the Mj after infecting the *minmad-1* transgenic tobaccos was significantly higher than that of the control. (*H*) The genomic DNA 6mA content of the Ma 4n after infecting the *minmad-1* transgenic tobaccos was significantly higher than that of the control. *p* values were calculated by two-tailed unpaired Student's *t*-test. One star * means $p < 0.05$, two means $p < 0.01$, three means $p < 0.001$.

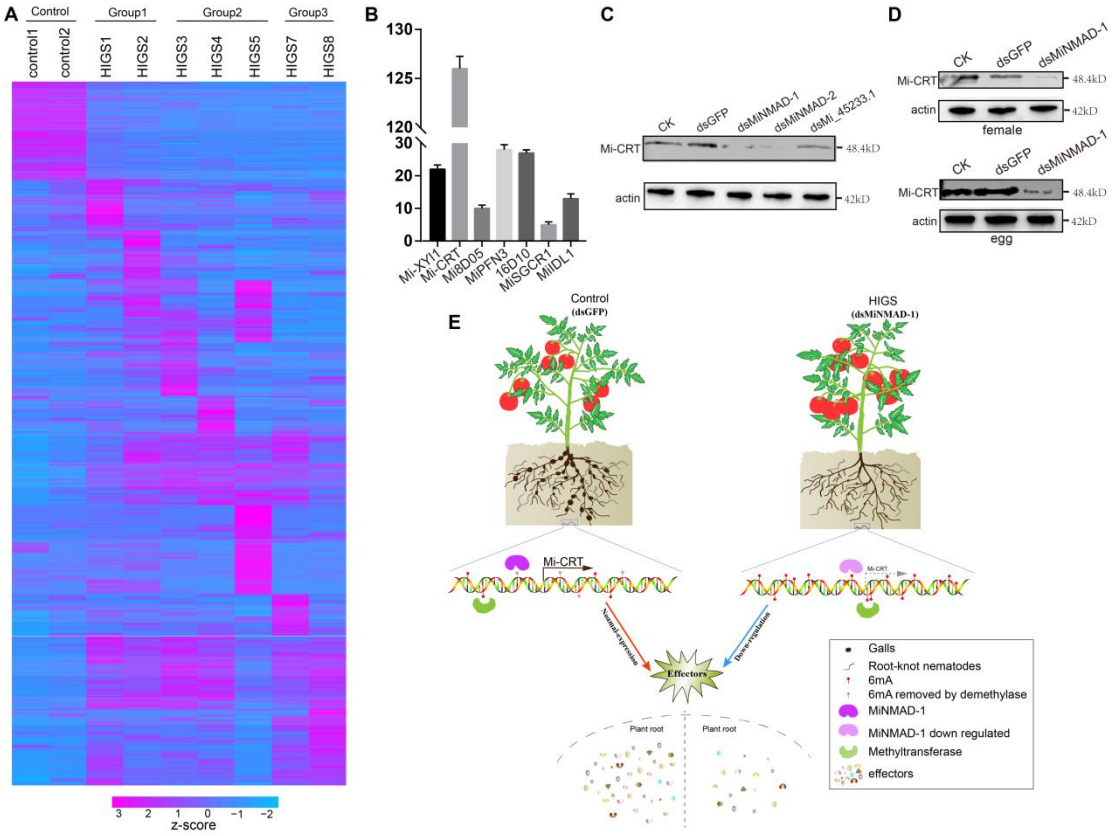

Figure 6. 6mA regulation of the expression module of *M. incognita* effector. (*A*) The Expression patterns of all secreted proteins at Mi J3J4 stage in dsGFP control group and *minmad-1/2* RNAi group. Group1: multiple-galls. Group2: medium-galls. Group3: low-galls. (*B*) Relative fold down-regulation of some validated effectors after HIGS of *minmad-1*, assay was performed by qRT-PCR in Mi female. (*C*) Western blot of the highest down-regulate effector show that Mi-CRT was also significantly down-regulated at the protein level after *minmad-1/2* RNAi. (*D*) Mi-CRT protein level down-regulate both at egg and female stage. (*E*) Schematic illustration of the regulation of Mi virulence factor expression patterns by 6mA to affect the ability of nematode infectivity.